NASA-CR-194193

SECA-TR-91-8

RELEASE DATE 6-6-93

LOW ALTITUDE PLUME IMPINGEMENT HANDBOOK

SBIR-02.08-8581A

Contract No. NAS8-38423
Purchase Orders 1504, 1575, 1633, 1688, and 1808

Prepared for:

REMTECH, Incorporated
3304 Westmill Drive
Huntsville, AL 35805

By:

Sheldon D. Smith

SECA, Inc.
3311 Bob Wallace Avenue
Suite 203
Huntsville, AL 35805

August 9, 1991

Contents

List of Figures

List of Tables

NOMENCLATURE

Al%	=	percent aluminum by weight
C_p	=	specific heat
D	=	diameter
g	=	gravitational constant
h	=	heat-transfer coefficient
i	=	enthalpy
Le, M	=	Lewis and Mach numbers, respectively
$\dot{m}$	=	mass flow
P	=	pressure
Pr	=	Prandtl number
q	=	dynamic pressure = $\rho u^2/2$
$\dot{q}$	=	heat flux; $\dot{q}_c$, convective; $\dot{q}_r$, radiative
R	=	gas constant
Re	=	Reynolds number
r	=	radius or radial flow length
$r_{1/2}$	=	radius at the half velocity
T	=	temperature
u	=	velocity
X	=	axial distance from nozzle exit
β	=	velocity gradient
γ	=	specific heat ratio
μ	=	viscosity
ρ	=	density
Φ	=	axial moment; $\Phi_t = 2\pi \int_o^\infty \rho u^2 r\, dr \equiv \gamma P_\infty M_{opt}^2 A_{opt}$
Subscripts		
c	=	chamber (or convective, with $\dot{q}$)
cc	=	constant core
cl, cw	=	centerline and cold wall, respectively
D	=	dissociation
e, ex	=	jet edge and exit, rspectively
g, i	=	gas and plate flow, respectively
k	=	kth ring in plate flow analysis
opt	=	optimum (after isentropic change from P_{ex} to P_∞)
R, s	=	recovery and stagnation, respectively
r	=	plate radius
ss, sup	=	sonic tip and supersonic, respectively
t, w	=	total and wall, respectively
2,∞	=	downstream of shock, and ambient, respectively

Section 1
INTRODUCTION

Plume Impingement modeling is required whenever an object immersed in a rocket exhaust plume must survive or remain undamaged within specified limits, due to thermal and pressure environments induced by the plume. At high altitudes inviscid plume models (RAMP2,[1], MOC [2]), Monte Carlo techniques [3–5] along with the Plume Impingement Program can be used to predict reasonably accurate environments since there are usually no strong flowfield/body interactions or atmospheric effects. However, at low altitudes there is plume-atmospheric mixing and potential large flowfield perturbations due to plume-structure interaction. If the impinged surface is large relative to the flowfield and the flowfield is supersonic, the shock near the surface can stand off the surface several exit radii. This results in an effective total pressure that is higher than that which exists in the free plume at the surface. Additionally, in two phase plumes, there can be strong particle-gas interaction in the flowfield immediately ahead of the surface.

To date there have been three levels of sophistication that have been used for low altitude plume induced environment predictions. Level I calculations rely on empirical characterizations of the flowfield and relatively simple impingement modeling. An example of this technique is described by Piesik in Refs. [6,7]. A Level II approach consists of characterizing the viscous plume using the SPF/2 code [8] or RAMP2/LAMP [9] and using the Plume Impingement Program to predict the environments. A Level III analysis would consist of using a Navier-Stokes code such as the FDNS code [10] to model the flowfield and structure during a single calculation. To date, Level I and Level II type analyses have been primarily used to perform environment calculations. The recent advances in CFD modeling and computer resources allow Level II type analysis to be used for final design studies. Following some background on low altitude impingement, Level I, II and II type analysis will be described.

Section 2
BACKGROUND

The most important ingredient in determining the plume induced environments to launch stands is an accurate description of the launch vehicle or missile plume flowfields. At low altitudes the rocket engine exhaust plume is dissipated by the entrainment of the relatively low energy ambient atmosphere into the high velocity exhaust products. In order to properly characterize plume environments to launch stands, deflectors and adjacent hardware, the mixing of the exhaust plume and ambient atmosphere must be considered. Figure 1 illustrates the necessity of including mixing in low altitude plume predictions. Figure 1 presents the centerline pitot total pressure distribution for the Space Shuttle Solid Rocket Motor (SRM) calculated with and without mixing. The dashed line is the inviscid calculation and the solid line is the results of a calculation including mixing. Beyond 200 ft the inviscid results are much too conservative.

Launch Stand environments for the Saturn [11,12] and Space Shuttle [13,14] utilized a method by which the inviscid and viscous flowfields were calculated separately, then manually merged to generate a composite flowfield which was then used to define the environments. The inviscid flowfields for the Saturn and Shuttle liquid engine exhaust plumes were calculated using single phase (i.e., gas only) Method of Characteristics codes [2], while the Space Shuttle SRM inviscid plume was calculated using the Reacting and Multiphase Program (RAMP) [15] which treated two-phase (gas and particulates) flow effects. RAMP2 and MOC calculations are initiated at the throat of the engine based on the results of combustion chamber and transonic analysis for starting conditions. These calculations include the effects of equilibrium chemistry and in the case of RAMP, the exchange of energy and momentum between particles and gas (for solid rocket motors). The inviscid flowfields are calculated to distances in the plume beyond which the ambient atmosphere would mix to the plume axis.

The viscous portion of the Saturn and Shuttle plumes were calculated with models [9,16] that utilize a forward marching finite difference method that solve the boundary layer form of the governing equations.

The initial conditions used for the mixing calculations were obtained by averaging the exit plane gas properties as calculated by RAMP2 and one dimensionally expanding or compressing them to atmospheric conditions.

The turbulent shear stress model used for Shuttle calculations was the two-equation TKE model of Launder et al. [17]. This model was chosen based on previous work presented in Ref. [13] which used this TKE model to compare with model engine data similar in Mach number and density ratio to the SRM sea level plume. The Saturn calculations utilized eddy viscosity models since the newer TKE models were not developed at the time.

At the time of the initial Space Shuttle Plume and Launch Stand environment studies, the mixing codes would not treat two-phase flow in a coupled manner. The overall model which was developed for Shuttle Launch complex [18] for SRM impingement used the

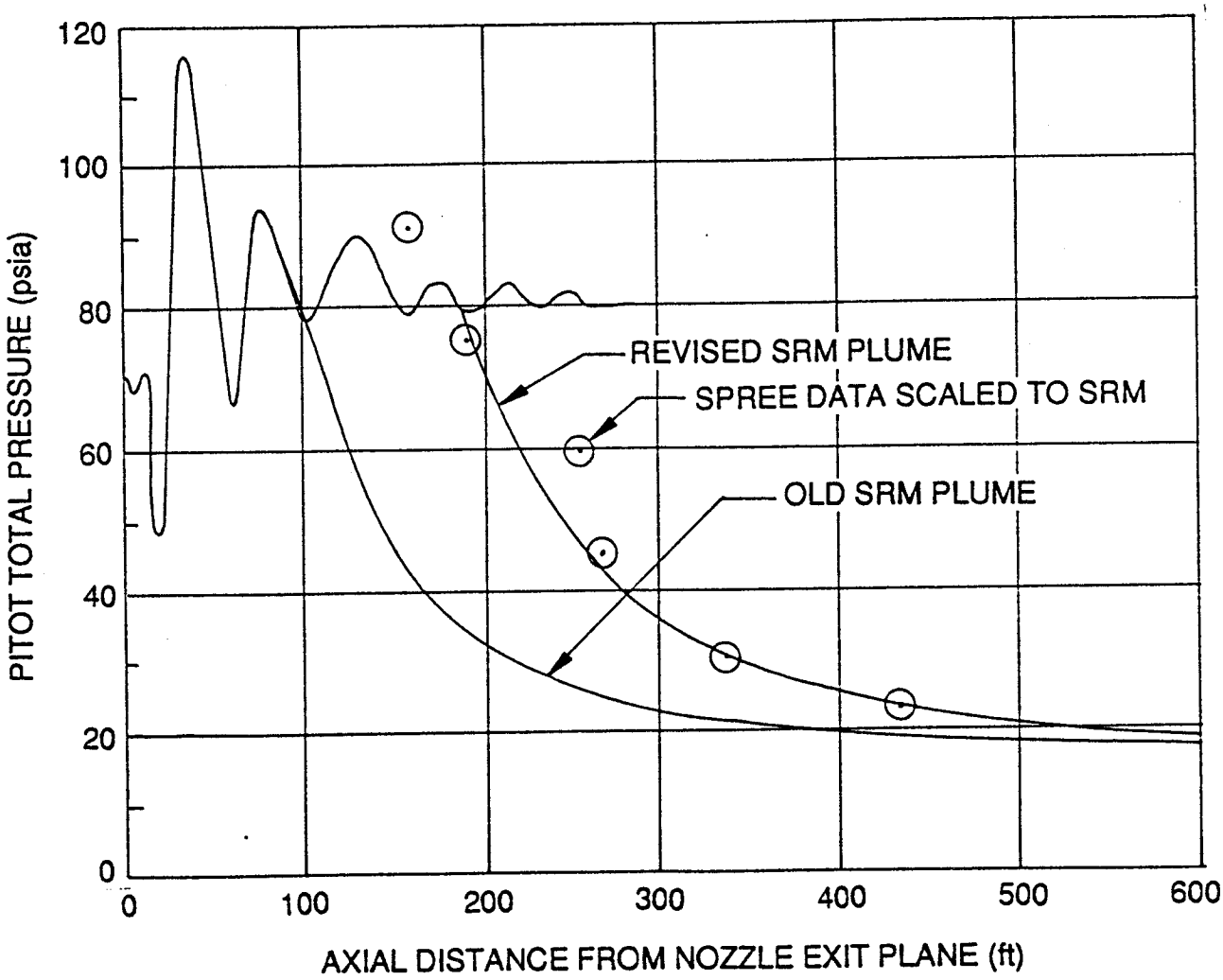

Figure 1: Space Shuttle Solid Rocket Motor Exhaust Plume Centerline Pitot Total Pressure Distribution at Sea Level

assumption that the particles in the mixing region were at the same temperature and velocity as the gas and diffused at the same rate as the gas. While thermal and dynamic equilibrium of the particles and gas is probably not a bad assumption many nozzle exit diameters downstream of the exit, in the region between the inviscid portion of the plume down to about 25 diameters from the exit, the particles will in reality not be in equilibrium with the gas. The overall model [18] which was used for the Space Shuttle Launch environments was validated against a limited amount of heat transfer data as well as a good deal of pressure data. Part of the model included factors such as accommodation coefficients which account for how most of the particulate energy is transferred to an impinged surface. These factors were determined based on the above mentioned data and plumes which were calculated in the same manner as the SRM. The model used for the Space Shuttle Launch Stand environment was fairly well validated but it is uncertain how the assumption of gas-particle equilibrium in the mixing region affects some of the empirical factors that were determined based on the model validation studies.

Subsequent to the previously mentioned modeling of inviscid/viscous flows, a new model has been developed that will greatly reduce the labor required to model a low altitude plume. The Standard Plume Flowfield code (SPF/2) [8] has been developed under joint government funding of the Joint Army-Navy-NASA-Air Force (JANNAF) committee. The SPF/2 code was envisioned as a standardized program which can treat all of the important plume effects at low altitudes. The primary emphasis in the SPF/2 development was for application to radiation signatures. However, the code can be used to provide plume characteristics for plume impingement environments. Table 1 (taken from Ref. [8]) gives a summary of the features and capabilities of the SPF class of programs. SPF/1 was the original code which has been replaced with SPF/2. SPF/3 which utilizes parabolized Navier-Stokes methodology is still under development but could be readily used for plume impingement applications when it is fully developed and validated. SPF/2 is comprised of three separate programs: PROCESS, SKIPPY and BOAT. The PROCESS module sets up the input files for the SKIPPY and BOAT codes. SKIPPY solves the inviscid flowfield starting at the exit plane and will treat the Mach disc regions and two-phase flow assuming frozen chemistry (uniform gas species distribution). The BOAT code calculates the mixing portion of the plume. The BOAT code will treat two-phase flow and includes finite rate chemistry which is important in low altitude plumes where afterburning may raise the temperature in the mixing layer due to the combustion of the fuel rich exhaust products and air. The BOAT code has the advantage over the earlier mixing codes in that the properties at the inner edge of the shear layer are automatically varied using the results of the inviscid SKIPPY calculation, so that an exact match of the inviscid/viscous results is obtained for both gas as well as particulates. Figure 2 gives a schematic representation of a SPF/2 plume. The distribution of gaseous and particulate properties at the exit plane of the motor are input to the SPF/2 code. The RAMP2 code which was developed under NASA funding has been modified to output a file which contains the exit plane data which is in the proper format for input to the SPF/2 code.

Table 1: Features of SPF/1, SPF/2 and SPF/3 [8]

VERSION	NEARFIELD	TRANSITION REGION	FARFIELD	KEY FEATURES/LIMITATIONS
SPF/1	Mixing Overlaid on Inviscid Map	Mixing with Prescribed Pressure Decay	Constant Pressure Mixing	• Single-phase flow • No Mach disc mixing/chemistry • Uniform composition exhaust • Finite rate chemistry in mixing solution • Initial plume expansion angle ≤ 70°
SPF/2	Plume Mixing Layer Overlaid on Viscous/ Inviscid Map Containing Mach Disc Mixing Solution	As above; Plume and Mach Disc Mixing Layers Merged	Constant Pressure Mixing	• Single- and two-phase flow • Mach disc mixing • Uniform composition exhaust • Finite rate and equilibrium chemistry options in mixing solution • Initial plume expansion angle > 90°
SPF/3	Fully-Coupled Parabolized Navier-Stokes Solution		Constant Pressure Mixing	• Single- and two-phase flow • Mach disc mixing/chemistry • Uniform composition exhaust • Finite rate and equilibrium chemistry options in mixing solution • Initial plume expansion angle > 90°

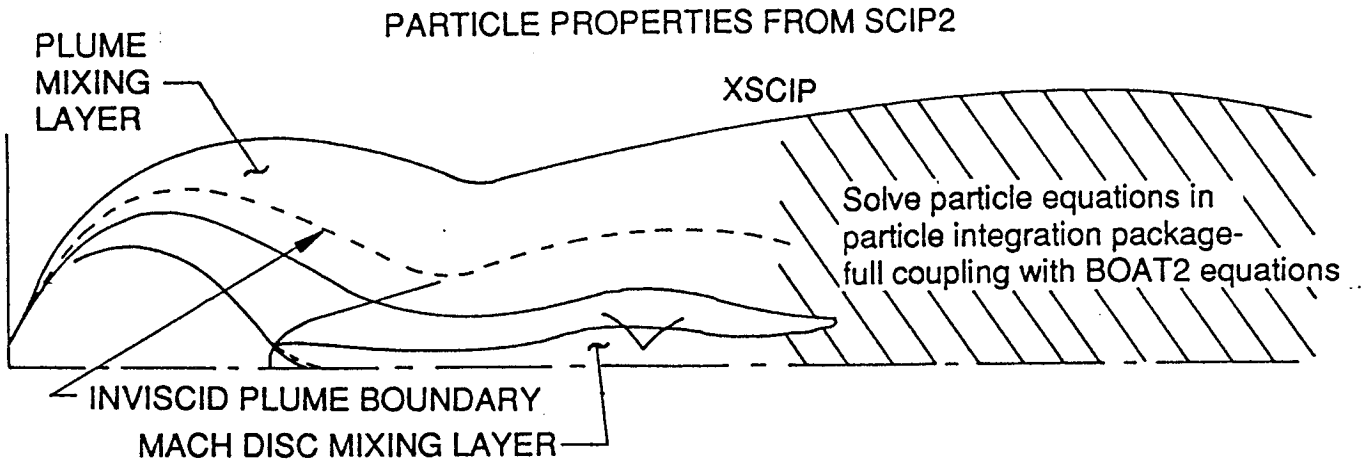

Figure 2: Schematic of SPF/2 Gas/Particle Overlaid Procedure

The Plume Impingement Program (PLIMP) which was funded by NASA is widely used for predicting plume impingement induced forces, moments, heating rates and contamination to bodies immersed in the flow of liquid and solid rocket plumes. PLIMP uses a free body concept whereby a plume is precomputed, the body is located in the plume, and appropriate shock and heating theory is used to determine impingement pressures and forces. PLIMP has numerous options for modeling geometries that are very applicable to launch complexes. Additionally, the way it is configured allows the user to set up the geometry one time then move the engine relative to the impinged surfaces to simulate the movement of the launch vehicle or missile relative to the launcher. Improvements in the PLIMP theory that are necessary to model low altitude impingement will be addressed under the Level II analysis described in Section 4.

As was mentioned in Section 1, Navier-Stokes codes have been developed to the level that they can be utilized to produce low altitude plume induced environments. Three dimensional Navier-Stokes codes can model both the plume flowfield and the disturbed flowfield in the vicinity of the impinged body since the body geometry can be simulated by the codes via boundary conditions. For solid rocket motor plumes, the ability of the CFD codes to calculate the interaction of particulates and gas in the shock layer adjacent to the body is of particular interest since the actual particle fluxes (momentum and energy) which strike the surface are calculated.

Traditionally, the amount of particulate incident energy which is transferred to the surface is treated using an accommodation coefficient. Usually, the accommodation coefficient accounts for the particle-gas interaction in the shock layer, the shielding of the surface by the particle debris layer and the time the particles actually interact with the surface and transfer energy. It is easy to see that the accommodation coefficient can change radically for the same plume depending on the orientation, size and incident mass flux of the particles. Thus, in order to be conservative for all impingement scenarios a relatively high (0.5) accommodation coefficient must be used. Previous studies [19] have attempted to determine accommodation coefficients as a function of incident particle mass flux for a particular impingement geometry. The resultant correlation was fairly good. However, the same correlation may or may not be applicable to other geometries,

orientations, and motors. Navier-Stokes codes now provide a model that can possibly be used to determine a realistic accommodation coefficient/particle incident mass flux dependence that can be used to determine two-phase impingement heat loads.

The FDNS code which is under development for NASA is a two-phase Navier-Stokes code which can treat ideal, equilibrium, frozen or finite-rate chemistry. This code uses a Lagrangian particle trajectory scheme. Recently, it has been applied to solid rocket motor impingement scenarios. The FDNS code can be used for environment predictions that require a Level III analysis. Section 5 will discuss the FDNS code and applications which have used the model.

Section 3
LOW ALTITUDE PLUME/PLUME IMPINGEMENT MODELING

Level I plume/impingement models are considered to be simple semi-empirical methods that can be used to provide preliminary design environments for relatively simple geometries. These methods should be easily programmable on personal computers and run in seconds. An excellent example of this type technique was developed by Piesik and is described in Refs. [6,7]. Excerpts of these two papers are used in the following discussion to describe the model. Complete details of the model can be found in Refs. [6,7].

Piesik's model uses semi-empirical methods for the prediction of the pressure and heat transfer effects of a stationary (or slowly moving) rocket impinging normally on a flat surface at sea level. He divides the problem into three parts.

1. definition of the flow parameters of the free exhaust (which may be anywhere from overexpanded to moderately underexpanded) by use of empirical relations for the centerline variations of the parameters and Gaussian distribution to describe radial distributions;
2. definition of the flow parameters on a flat surface resulting from normal impingement of the free exhaust; and
3. the heat-transfer definition using the plate flow model parameters and the well-known heat-transfer equations of Fay and Riddell, and Van Driest.

3.1 Free Exhaust Flowfield

It is assumed that P_c, T_c, R, γ, D_{ex}, and M_{ex} are known, and that the static pressure in the exhaust flowfield is everywhere equal to the ambient pressure (P_∞ = 14.7 psia). Further assumptions which are made are:

1. The momentum of the exhaust after expansion or compression to ambient pressure is conserved.
2. Metal oxides in the exhaust species are considered to be in the gaseous state in thermal and dynamic equilibrium with the gas
3. No shock structure is considered in the supersonic portion of the plume.
4. The supersonic flow of the plume decays smoothly as an exponential function:

The descriptions of the centerline distributions of recovery pressure and temperature in the subsonic region of the plume were generated based on a wide range of experimental data. First, the location of the sonic tip is located. The sonic tip is a function of exit Mach number, pressure, and jet diameter expanded to the ambient pressure (M_{opt}, P_{opt}, D_{opt}), specific heat ratio and ambient pressure. The Mach number distribution up to the sonic tip is an exponential function of the M_{opt} and the sonic length.

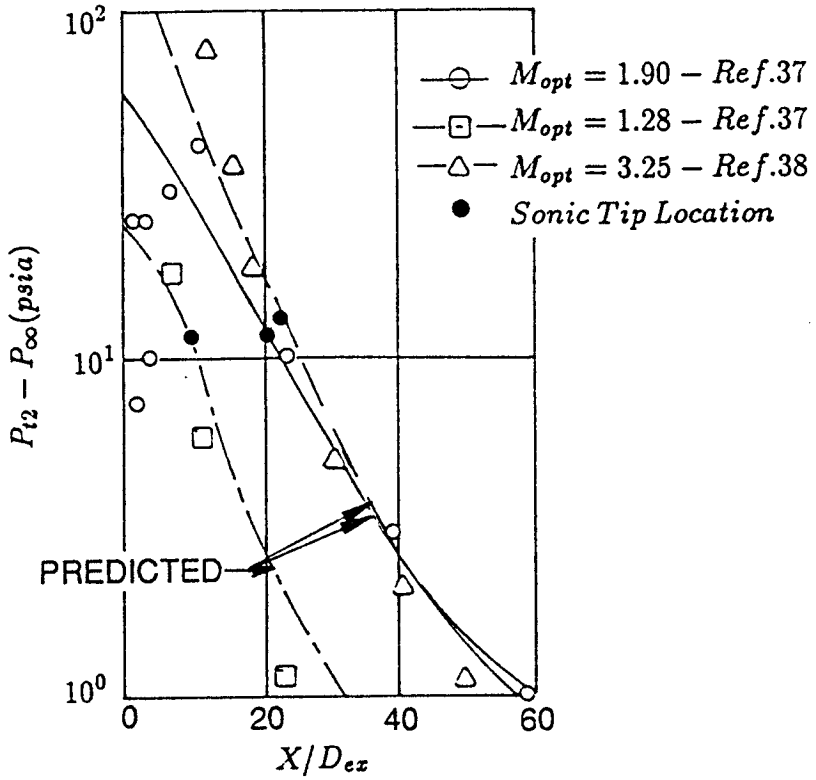

Figure 3: Centerline Recovery Pressures

The centerline length of the inviscid region is calculated based on the sonic length and the percent loading of aluminum. The original formulation of this model did not include effects of Al loading but the new model presented in Ref. [7] includes this effect and does a better job of describing solid motor plumes. Next, the centerline pitot pressure in the subsonic portion is calculated as a function of X, D_{opt}, M_{opt}, P_{topt}, P_∞ and the sonic length. The total temperature is calculated as a function of sonic length, inviscid length, Al loading, D_{opt}, T_c, and ambient temperature.

Figures 3 and 4 present typical results of comparisons of Piesik's centerline model with experimental data. Figure 3 presents pitot pressure distributions and Fig. 4shows total temperature distribution. These comparisons are fairly good in the decaying portion of the plume. However, in the core region, the model will either under- or overpredict the total pressure due to shock or compression wave, but on the average the model produces reasonable results.

The radial distribution is calculated starting with the assumption the total momentum in the flow is conserved and is equal to the momentum of the jet after it has expanded to ambient conditions. It is further assumed that the flow properties in the core region at any particular axial location do not vary in a radial direction. The radius of the core flow is a function of M_{cl}, r_{opt} and M_{opt}. The velocity distribution in the mixing region is calculated using a Gaussian distribution and the conservation of momentum.

In the mixing (subsonic) region, Fig. 5, the radial distribution of the mass fraction of ambient air $\alpha = \alpha(r)$, at a particular station (X) is assumed to be dependent upon the momentum distribution. The gas properties (T_t, T, γ) required for the flowfield predictions

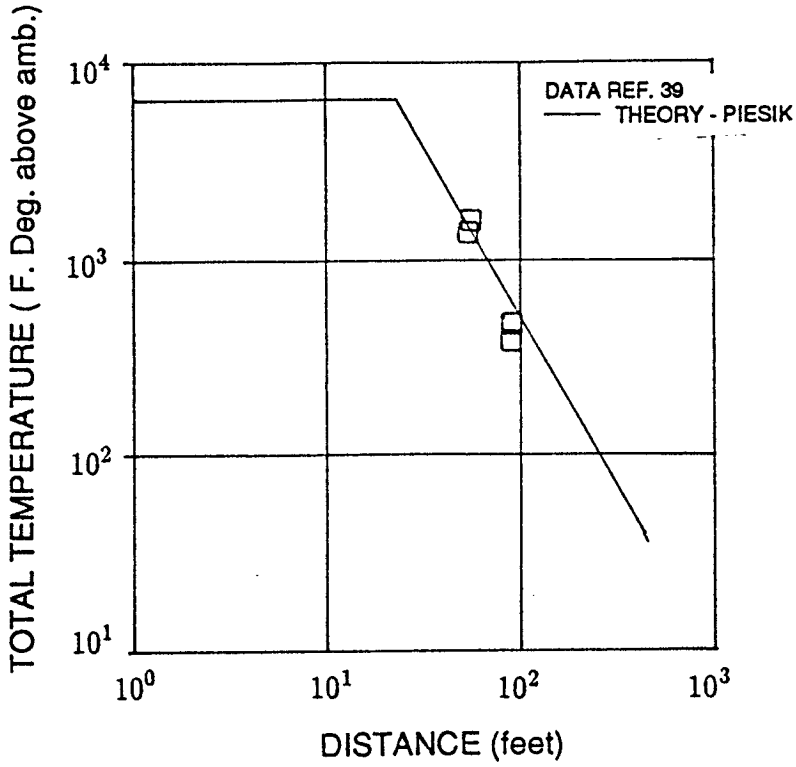

Figure 4: MK104 DTRM, Total Temperature Comparison, Centerline, 22% Aluminum

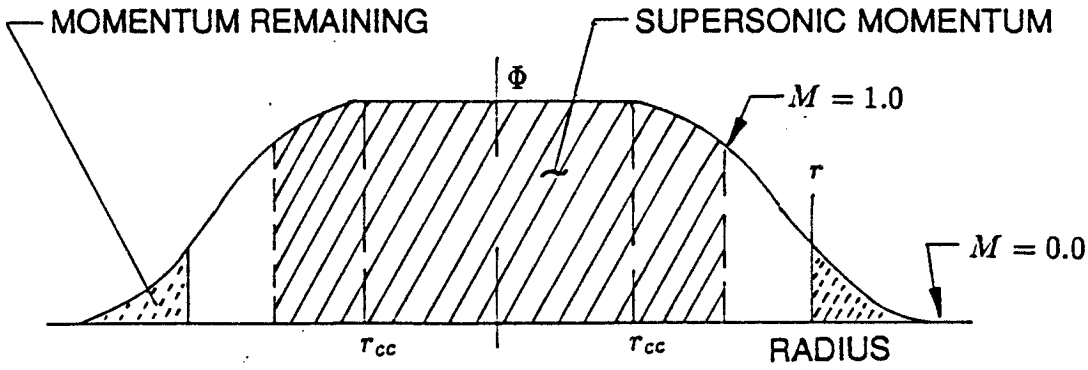

Figure 5: Mixing Region Model

at any radius in the subsonic region are taken as the bulk averages of the exhaust/air constituents.

Figures 6 and 7 present radial distributions of calculated and measure pitot pressure and total temperature for a 22% Al motor 73 radii downstream of the exit. Calculations using this model, SPF/2 and data are shown. In general, this model does a reasonable job in predicting the radial distributions for far field mixing. SPF/2 tends to underpredict pitot pressure. Part of this underprediction by SPF/2 could be accounted for by using a different mixing model. However, for highly aluminized motors, SPF/2 tends to underpredict pitot pressure near the centerline in the core of the plume. This will be further discussed in Section 4.

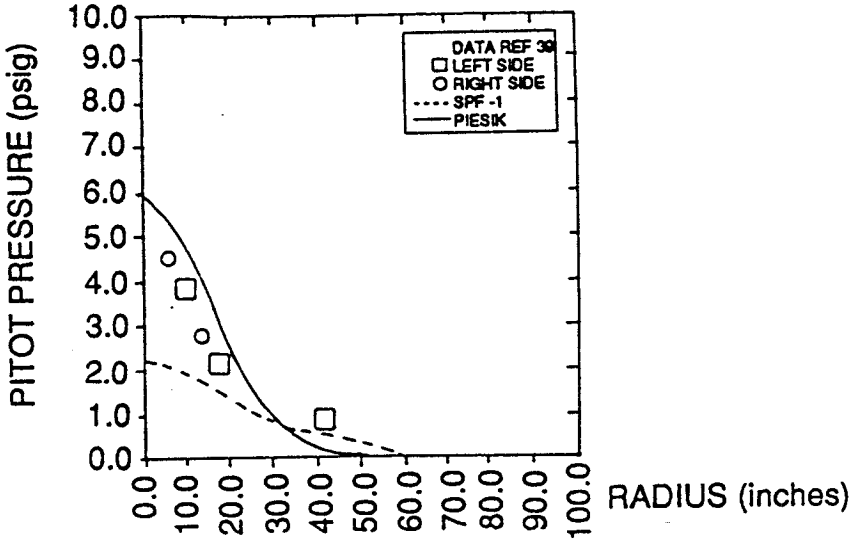

Figure 6: MK104 DTRM, Pitot Pressure Comparison, X=40 Ft, 22% Aluminum

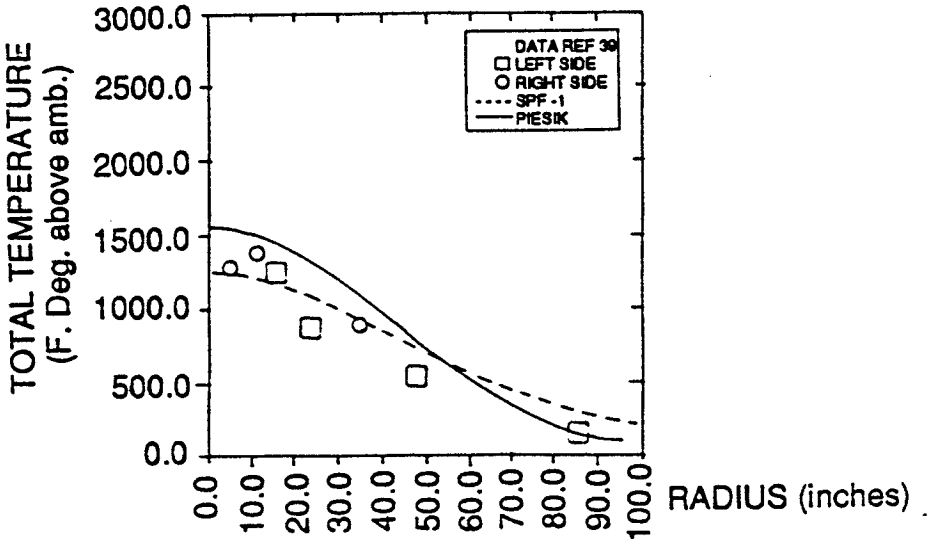

Figure 7: MK104 DTRM, Total Temperature Comparison, X=55 Ft, 22% Aluminum

3.2 Flat Plate Flow

The flow parameters parallel to the flat plate after the normal impingement of the exhaust are based upon a simple mixing theory. It is assumed that at any radial location in the free exhaust the flow approaches the plate (negotiating a normal shock where necessary) and instantaneously turns parallel to the plate, completely mixing with any plate flow up to that location. It is further assumed that the $P(r)$ on the plate can be closely approximated as being equal to the free exhaust's $P_{t2}(r)$. This assumption is consistent with observations of experiments for normal flat plate impingement especially when the flow is fully mixed.

The flow parameters on the plate are readily determined from the gas-dynamic relations and the equation of continuity as one allows the impinging normal flow to be divided into concentric rings, $k (k = 1,2, \ldots n)$ which are thin enough that the flow parameters can be considered constant within each ring. Starting at the center, the flow across the radial boundary of each ring is calculated. Mach number along the plate surface is determined using the free-exhaust $P_{t2}(r)$ and the $P_t(r)$ of the flow along the plate. Remember that $P(r)$ on the plate is equal to $P_{t2}(r)$. Thus $P_t(r)$ along the plate is composed of the partial pressure of the flow on the plate up to that ring plus the partial pressure of the flow coming into the ring from the free exhaust.

The $T_t(r)$ of the plate flow is the bulk average of all flow rings from the jet centerline up to and including the ring, k, in question. Similarly, $\dot{m}(r)$ is simply the total mass flow for all rings through ring, k. With M_k and T_{tk} defined, T_k and u_k are easily obtained.

3.3 Heat-Transfer Analysis

For convective heating, the gas impinging on the flat plate can be divided into three regions (Fig. 8) which require slightly different treatments: (1) the exhaust core

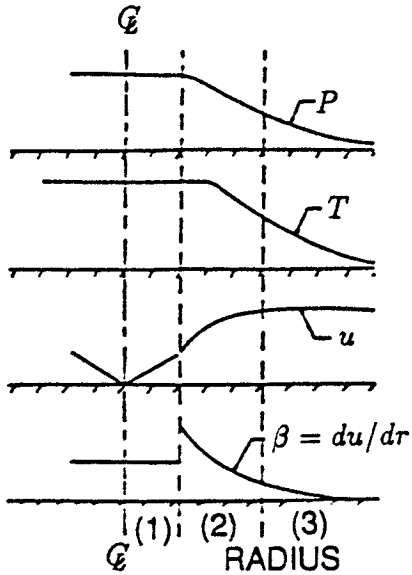

Figure 8: Flow Region for Flat Plate Heat Transfer

impingement region, (2) the region of high pressure gradient dP/dr just outside the core, and (3) the essentially constant-pressure region at large distances from the jet axis. In region 1 (which is of concern only when the plate is located at $X < X_{SS}$), the free exhaust flow properties, u, P, and T, are constant at each X. It is assumed that the velocity gradient on the plate ($\beta = du/dr$) is constant in this region, so the heat-transfer coefficient, h, varies only with distance, r, from the center. In region 2, the flow is rapidly accelerated, so that β is high and varies rapidly. In region 3, $P_{t2} \rightarrow P_\infty$, and u is nearly constant, but at great distances begins to decline; this is similar to constant velocity flow over a flat plate.

Two equations are used to predict q_c for the entire flowfield. For q_{ccl}, the laminar stagnation region equation of Fay-Riddell [20] is used. Otherwise, q_c is predicted using the Van Driest equation for turbulent stagnation region heating. It is necessary only to modify the β term in each of the three defined flow regions.

Figure 9 presents calculated cold wall centerline heat rate distribution (including measured radiant heat flux) compared with experimental total heat flux for scale model liquid rocket engine impingement. In general, the comparison is quite good (±30%). Figure 10 presents flat plate impingement heating rate data and calculations for a 22% Aluminized motor. Two measurements are shown. The data is presented as hot wall heating rate vs. time. For this case the predicted values are ±100% and the integrated heat loa is +40, −0. This is understandable, since Al_2O_3 impingement is treated as a gas. The model could be improved by assuming that the Al_2O_3 is a particulate and is in thermal and dynamic equilibrium with the gas and comprises a fixed percentage of the flow. Then particle kinetic and thermal energy fluxes can be calculated. Finally, by multiplying these fluxes by an accommodation coefficient, the actual particulate heat flux could be calculated.

The overall model described in this section is fairly simple and can be used to generate preliminary design numbers. If the uncertainties in this type of an analysis are unacceptable for design, then it would be necessary to use a Level II or Level III analysis.

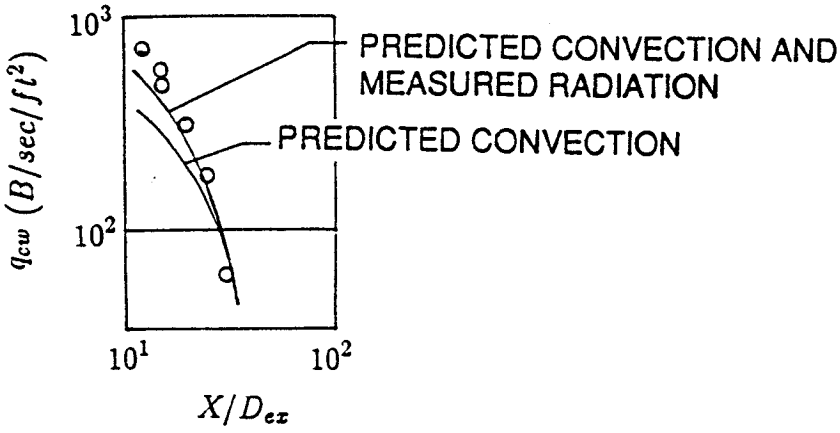

Figure 9: Centerline Heat Flux Comparison

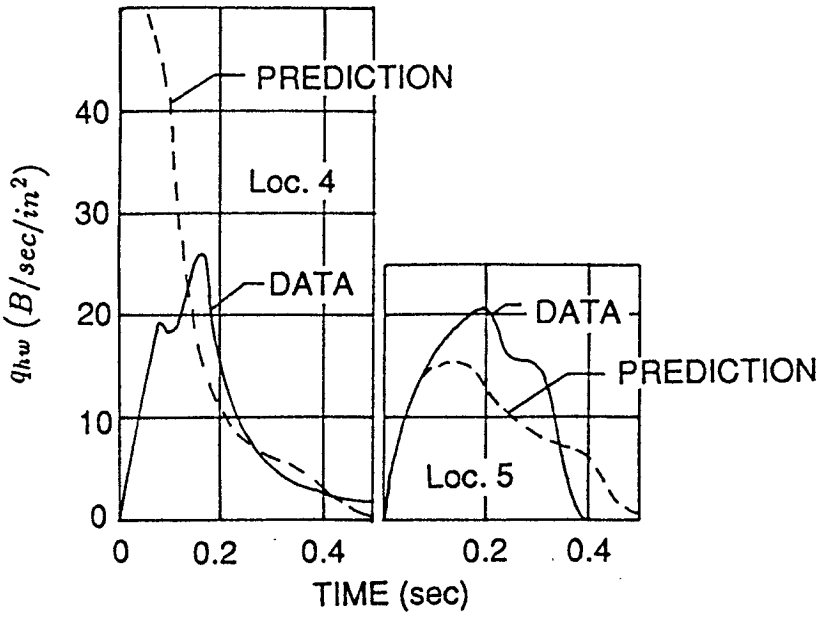

Figure 10: Aluminized Solid-Propellant Heat Flux

Section 4
LEVEL II IMPINGEMENT ANALYSIS

A Level II low altitude impingement analysis would consist of using a viscous flowfield code such as SPF/2 and a separate impingement modeling code such as the PLIMP code. This section of the appendix will describe the interaction of SPF/2 with PLIMP, present a simple analysis and finally describe modeling which is required for low altitude solid rocket impingement heat transfer analysis.

4.1 SPF/2/and PLIMP Models

SPF/2 calculates all the necessary information that can be used by PLIMP to determine pressures and heating rates. However, PLIMP was previously set up to handle the thermodynamic and flowfield data generated by the RAMP and MOC programs. Recently SPF/2 and PLIMP have been modified so that impingement calculation can be made using the SPF/2 flowfield [21].

SPF/2 uses a Cartesian coordinate system with the data surfaces normal to the centerline of the engine. The solution is a forward marching scheme with the flowfield calculated starting at the exit and progressing downstream to the problem limits. As was previously mentioned, SPF/2 was originally intended to be used primarily for radiation applications and one of the options in the code is to output a file that can be used by the Standard Infrared Radiation Model [22,23] to perform radiation calculations. SPF/2 has several subroutines that are used to merge the SKIPPY inviscid and BOAT viscous flowfields for output to SIRRM. However, the data output in this file is not sufficient for the requirements of PLIMP. There was also a limitation of 50 total flowfield points that could be output at each solution station. Since it is possible to have as many as 75-80 points when merging the SKIPPY and BOAT flowfields, this limitation was eliminated from the new modified version of SPF/2 so that the entire flowfield is output. Modifications were made to several subroutines [BOATII, BOATIP, BOATJT, BOATOT, PARTOT, PITOT (new)] in the BOAT module to generate the output flowfield in a manner which was generally consistent with the format of the RAMP code so that modifications for input of the flowfield to PLIMP could be minimized. All the gaseous as well as particulate properties were output on a file (Unit 21) for communication with PLIMP. Table 2 shows the organization of the data file. If at a later date any other user of the PLIMP code needed to interface another flowfield model with PLIMP, by configuring the flowfield code to output data in the same format, no modifications will be necessary to the PLIMP code to use the flowfield to perform impingement calculations. In order to generate the SPF/2 flowfield file during the BOAT mixing calculations NRAD (generates flowfield file for SIRRM) must be set = 1, on card 33 of Ref. [24] input guide. No other changes to the SPF/2 code or input are required to output the flowfield on File 21.

The modifications which were made to the PLIMP code during this effort were extensive. Besides making the modifications to the subroutines which read in the

Table 2: Description of Unformatted Binary Output of SPF/2 PLIMP Compatible Flowfield File (Unit 21)

GROUP I - General Information

Number of Records = 1

Write (21) (HEADER(I), I=1, 20), NS, ISPECS

- HEADER
  - problem descriptions (20A4)
- NS = number of gaseous species (25 max)
- ISPECS = number of particle species to be considered (10 max)

GROUP II - Finite-Rate Chemistry Species Names

Write (21) ((AID(I,LL),LL=1,2),I=1,NS)

- AID(I,1) first half of species number (A4)
- AID(I,2) second half of species name (A4)

Group II - Flowfield Data - One Set of This Group for each SPF/2 Output Station

Write (21) ITOT

- ITOT number of data points on the following vertical surface. If ITOT = O there is no information to follow

DO I=1, ITOT

Write (21) ITYPE,R,X,M,,S,μ,δ, Htg,V,PTOT,ρ,P,T,γ,Rc
I=1,ITOT

- ITYPE identifies type of point (wall, shock, interior, etc.)
  - 0 input point
  - 1 interior point
  - 2 wall point
  - 3 free boundary
- R radial coordinate (ft)

Table 2: (Continued) Description of Unformatted Binary Output of SPF/2 PLIMP Compatible Flowfield File (Unit 21)

- X axial coordinate (ft)
- M Mach number
- θ flow angle (rad)
- S entropy (ft^2/sec^2-°R)
- μ Mach angle (rad)
- δ shock angle (rad)
- Htg gas total enthalpy (ft^2/sec^2)
- V velocity (ft/sec)
- PTOT pitot total pressure (lbf/ft^2)
- ρ gas density ($slug/ft^3$)
- P pressure (lbf/ft^2)
- T temperature (°R)
- γ specific heat ratio
- R_c gas constant (ft^2/sec^2-°R)

Write (21) (SPECN,I=1,NS)

- NS number of gas species
- SPEN species mole fractions

*Write (21) ((U,V,T,H,ρ), J=1,ISP)

- ISP number of particle sizes at this point
- U axial velocity component (ft/sec)
- V radial velocity component (ft/sec)
- T temperature (°R)
- H enthalpy (ft^2/sec^2)
- ρ particle density ($slug/ft^3$)

END DO LOOP

*This record is written only for two-phase flowfields.

NOTE: The flowfield data are repetitively stored on tape as indicated above normal surface after normal surface. When ILAST = 0 the end of the data has been reached.

---

flowfield file, the PLIMP code had to be modified to be able to handle the thermodynamic properties and state variables in the same manner that the SPF/2 code uses them. Previous versions of the PLIMP program had the option of treating ideal gas plumes or plumes that were generated utilizing tables of one dimensionally expanded exhaust properties generated by the NASA Lewis Equilibrium Combustion Code (CEC) [25].

These tables allowed the RAMP2 or MOC flowfield to pass along only the independent variables (entropy, enthalpy and velocity).

Thus, any time the dependent variables (pressure, temperature, Mach number, species, etc.) were needed, the thermodynamic data tables and the independent variables could be used to determine them. The SPF/2 code however does not utilize a table lookup for the stated variables. The SPF/2 code has four chemistry options; ideal gas, frozen, equilibrium and finite-rate. Only the frozen or finite-rate options of SPF/2 are considered for inclusion into the PLIMP methodology since all previous as well as all anticipated future plumes will be calculated utilizing this option.

As was previously mentioned, the original version of PLIMP which was structured for the MOC and RAMP2 flowfields uses the independent variables ($O/F(H_T)$, V, and S) along with the thermodynamic data tables to determine the local flow properties and species at any given point in the plume. The SPF/2 code which uses the finite rate or frozen option calculates all the state properties and species mole fractions in a different manner so that much more information must be passed on to the PLIMP code in order to be able to do impingement calculations. The original PLIMP code only saved the first nine variables in Table 3, while the new version of the code has modifications that contain all the other variables that are shown in Table 3. In addition to the two ordered data files of the standard PLIMP code it was also necessary to add another file which contains the species mole fractions at each point in the flowfield. As each point is read in from the flowfield file during the ordering of the flowfield, the species mole fractions are sequentially written to Unit 4 and an index is added to the point. Thus, when the PLIMP code determines the local flow properties at any arbitrary point in the plume, the specie data can also be determined. Previously, the specie information was determined from the thermodynamic data on the format of the flowfield file, but now PLIMP can also determine species from flowfields which calculate species using other methodologies. One fallout of this modification is that PLIMP will be able to use a RAMP2 finite rate flowfield which it could not previously do.

The original PLIMP code could perform particle impingement force and heating rate calculations for two phase RAMP2 plumes. However, separate executions of the PLIMP code were required to do both gaseous and particulate calculations. A fallout of the modifications described in Ref. [21] is the ability to do both the gas and particulate calculations during a single PLIMP execution. This greatly reduces the amount of computer time and post processing of the data which was previously required when two executions were necessary. The last five variables shown in Table 3 are the particle property information necessary to calculate the force and heating rates to a body due to particulate impingement. The PLIMP particle impingement model is a simplified method for calculating particle effects to the surface. This simplified approach uses a user input accommodation coefficient to determine how much of the particle momentum and energy are actually transferred to the surface. The accommodation coefficient which has been determined experimentally accounts for the interaction of the particles in the shock layer and at the surface. The accommodation coefficient can vary over a significant range

Table 3: Representation of an Ordered Data Block

R	X	V	Θ	S	OF	M	TYPE	Θ_{rad}	T	ρ	R_M	γ	P_o^*	Θ_p	$(\rho V)_p$	$(\rho V^2)_p$	KE_p	TE_p
-	-																	
-	-																	
-	-																	
-	-																	
-	-																	
-	-																	
-	-																	
R_n	X	V	Θ	S	OF	M	TYPE	Θ_{rad}	T	ρ	R_M	γ	P_o^*	Θ_p	$(\rho V)_p$	$(\rho V^2)_p$	KE_p	TE_p

depending on the aluminum oxide loading (mass flux) and the shock layer ahead of the body. For calculations using the PLIMP version of the code a value of .5 is suggested. The existing version calculates the momentum transfer to the surface using Eq. 1 and heating rates using Eq. 2.

$$P_{impp} = \sum_{i=1}^{np} \rho_i V_i^2 \tag{1}$$

$$\dot{Q}_p = \alpha \, (TE + KE) \tag{2}$$

where

$$TE = C_{pp} \sum_{i=1}^{np} \rho_i V_i (T_i - T_{wall}) \tag{3}$$

$$KE = \sum_{i=1}^{np} 0.5 \, \rho_i V_i^3 \tag{4}$$

All heating rate, pressure and contamination options which exist in the PLIMP code for a RAMP or MOC flowfield are operational for a SPF/2 flowfield.

4.2 Application of the SPF/2/PLIMP Calculation for the Tomahawk LC39 Simulations

The set of data for which the SPF/2/PLIMP model was validated against was impingement pressure data taken during a test [26] that supported the design of the Space Shuttle Launch Complex 30. This test utilized a 20% Al Tomahawk Solid Motor [exit diameter — 8.5 inches, chamber pressure — 1000 (psia)] and a simulated Mobile Launcher Platform to determine the impingement pressure distribution at 12.2 and 17 ft from the Tomahawk exit plane (full scale shuttle of 214 and 298 ft). Two sets of calculations were performed using the SPF/2/PLIMP model.

The first set of calculations were performed using a two-phase SP/F/2 plume. The SPF/2 plume solution was started with a fully coupled exit plane startline determined from the RAMP2 solution of the Tomahawk nozzle. The results of the two-phase SPF/2 and plume impingement calculations of impact pressure for this case are presented in Figures 11 and 12. Figure 11 shows a comparison of measured and predicted impact pressures at 12.2 ft from the exit and Fig. 12 shows the results at 17 ft. The two-phase results underpredict the data at both locations. These results are similar to those observed in the pitot pressure correlations shown by Piesik [7].

The second set of SPF/2/PLIMP calculations was made using a SPF/2 plume which used the gas/particle equilibrium assumption. For this case the particulates are treated as a gas so that they stay in thermal and dynamic equilibrium with the gas. This is the same methodology that was used to develop the Space Shuttle Launch Complex plume

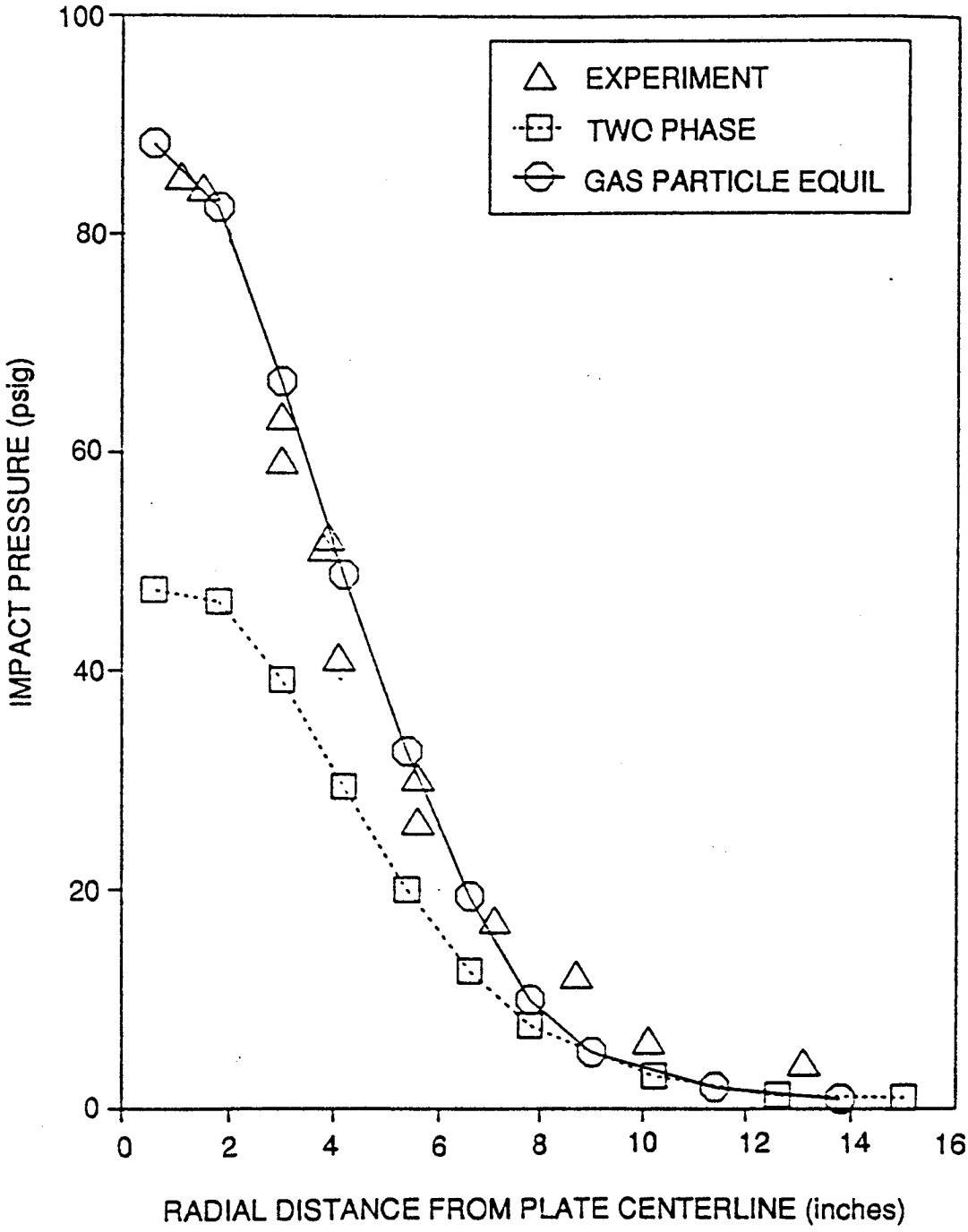

Figure 11: Comparison of Experimental and Calculated Impingement Pressure Distribution on Flat Plate 12.2 Ft from Exit Plane of Tomahawk Motor

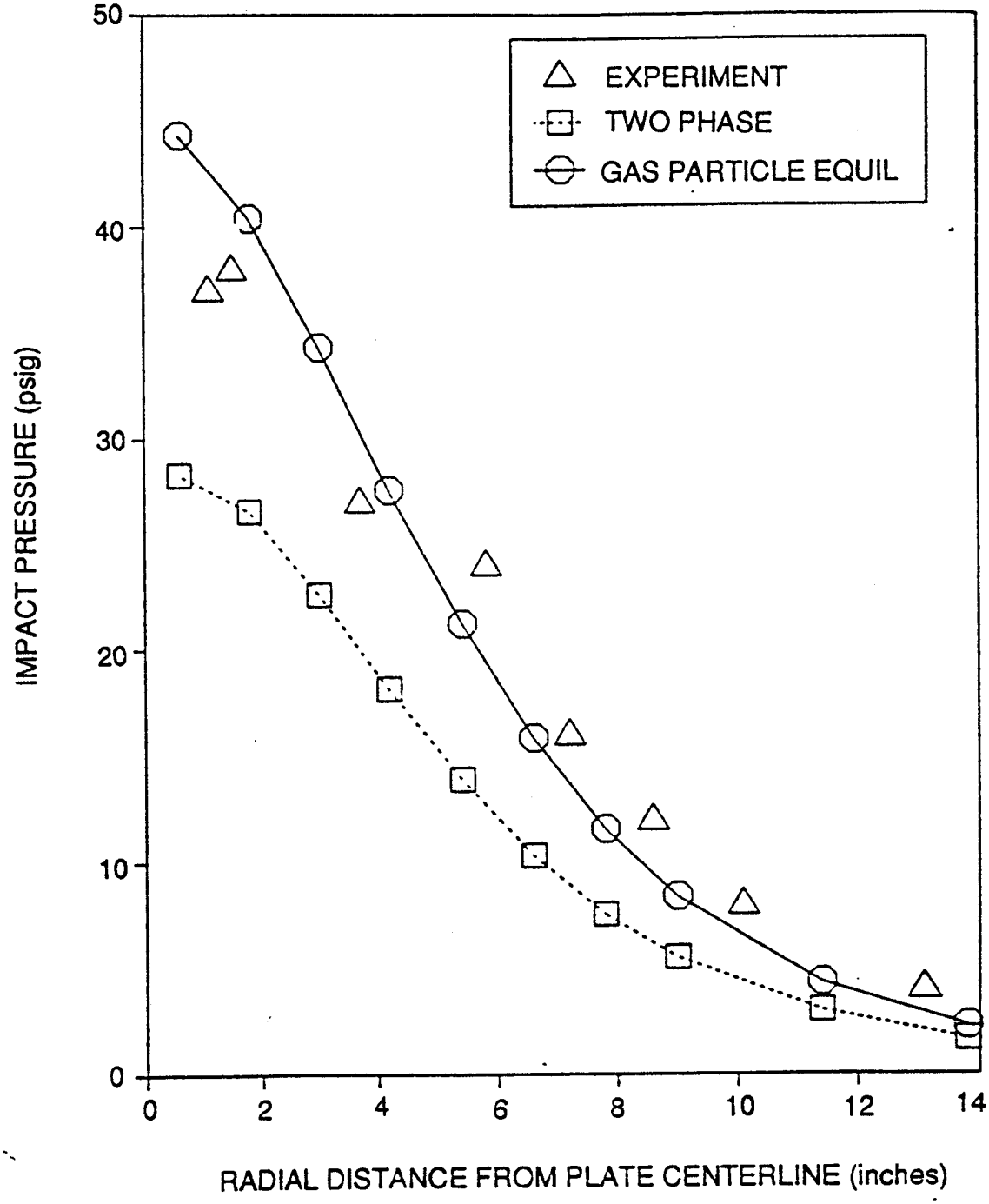

Figure 12: Comparison of Experimental and Calculated Impingement Pressure Distribution on Flat Plate 17.0 Ft from Exit Plane of Tomahawk Motor

induced environments described in Ref. [18]. This methodology including a heat transfer analysis will be further discussed in Section 4.4. The same exit plane startline was used to start the SPF/2 calculation except that the particulates were put back into the gas phase. Two-phase losses which occurred in the nozzle are included in the startline, but no further two-phase losses occur in the plume. Figures 11 and 12 also show the gas/particle equilibrium results. These impact pressure results compare very well with the data. One of the conclusions reached in specifying the environments [14,18] was that gas/particle equilibrium provided the best correlation with impingement pressures in the viscous portion of the plume. The SPF/2/PLIMP results assuming gas/particle equilibrium are consistent with previous findings. However, fully coupled two-phase calculations should be able to exactly predict the correct impingement pressures for two-phase impingement. It is possible that uncoupling the inviscid and viscous plumes for solid motors cannot adequately describe the flowfield and a fully coupled Navier-Stokes analysis such as a Level III calculation is necessary.

4.3 Sample Problem Using SPF/2/PLIMP Level II Analysis

A sample case for two-phase, low altitude, plume impingement is presented in this section. The sample case consists of a Space Shuttle Advanced Solid Rocket Motor (ASRM) plume impinging on the flame deflector. The deflector is a 32 ft long by 58 ft wide flat plate inclined 34 deg to the center of the ASRM plume, which has the nozzle 200 ft above the center of the deflector. An accommodation coefficient of .5 was used for the analysis. The input file is shown in Table 4. For demonstration purposes only, a single strip is calculated along the centerline of the deflector, using 5 points along the length of the deflector. For real calculations more strips and points should be used (say 40 points along 40 strips). Table 5 is a printed output of the results.

4.4 Description of a Low Altitude Plume/Thermal Response Model

This section describes a Level II type analysis that was performed to support the launch stand design for the Space Shuttle. There were three key areas that were addressed in order to develop an overall impingement model for the launch stand environments: (1) flowfield modeling, (2) model of the particle/gas interaction in the shock layer, and (3) a thermal response model of the structure. This model used another mixing code [9] along with RAMP and PLIMP, however the conclusions reached during the shuttle environment definition can be applied to a RAMP2/SPF/2/PLIMP analysis for future studies. References to RAMP/LAMP can be replaced with RAMP2/SPF/2. It is suggested that the hybrid mixing model (IVIS = −4) be used for low altitude plumes since plumes generated with RAMP2/SPF/2 using this model have similar characteristics as those calculated with RAMP/LAMP.

4.4.1 Plume Flowfield

The nozzle and inviscid plume flowfields were calculated using the RAMP program [15]. RAMP is a supersonic equilibrium chemistry two-phase flow code which

Table 4: Plume Impingement Program Input File for Low Altitude Sample Problems

```
    1    0    0    0    0    2
    1    0    0    0    0    0    2
0.0        0.0        0.0        1.0
   LC 39 ASRB FLAME DEFLECTOR
    1    0    3    1    0    1    0    0    2    0    0    1    1    1    0
200.0      0.0        0.0                                             0  123
0.0        0.0        124.
0.0        0.0        .1       -081.         1.0        1.0        1.0        0.0
2116.      540.       0.0         1.4        1716.      2.
.32         1.        0.0         2200.      .1333      1.0        .5          3DHM
540
32.        58.
200100500232.0        58.         0.0        0.0        0.0        0.0
0.0        0.0        0.0           123
0.0        0.0        0.0
0.0        0.0
100.       -100.      0.0         0.0        1000.       90.
END
```

Table 5: Plume Impingement Program Output File for Low Altitude Sample Problems

CASE NO. 1 PAGE 4

ROCKET EXHAUST PLUME IMPINGEMENT ANALYSIS USING THE LOCKHEED/HUNTSVILLE PLUME IMPINGEMENT COMPUTER PROGRAM

LC 39 ASRB FLAME DEFLECTOR

SUBSHAPE IN PLUME PARTICLE	IY RAD. CIRV. INFO	IZ SHADED	SHAPE REGIME Q-PARTICLE	X (SUBSHAPE) P IMPACT Q-TURBULENT P IMPACT(PAR)	Y (SUBSHAPE) IMPACT ANGLE REV. NO. (FT) IMPACT ANG(PAR)	Z (SUBSHAPE) PRESS. FORCE O TRANSIT PRESS FORCE(P)	PLUME X MASS FLUX-PLM O FREE MOLEC MASS FLUX-PLM	PLUME R P-STAT-PLM SHEAR STRESS KINETIC-PAR	MACH NO-PLUME ---- M-LOCAL THERMAL-PART
1	1	1	PLAT	0.00000E+00	-0.12800E+02	0.00000E+00	0.18939E+03	0.71577E+01	0.13846E+01
YES		NO	CONT	0.28306E+02	0.34512E+02	0.15131E+07	0.34479E+02	0.14617E+02	0.00000E+00
0.00000E+00		0.23623E+00		0.22036E+03	0.22000E+07	0.00000E+00	0.00000E+00	0.91334E-02	0.92621E+00
		0.44643E+04		0.51763E+01	0.35982E+02	0.27669E+06	0.86194E+01	0.38626E+04	0.11335E+05
1	2	1	PLAT	0.00000E+00	-0.64000E+01	0.00000E+00	0.19469E+03	0.35768E+01	0.18050E+01
YES		NO	CONT	0.37732E+02	0.34264E+02	0.20179E+07	0.42510E+02	0.14562E+02	0.00000E+00
0.00000E+00		0.24843E+02		0.33754E+03	0.84657E+07	0.00000E+00	0.00000E+00	0.99245E-02	0.11863E+01
		0.86651E+04		0.11678E+02	0.34668E+02	0.62421E+06	0.14640E+02	0.12346E+05	0.18121E+05
1	3	1	PLAT	0.00000E+00	-0.95367E-06	0.00000E+00	0.20000E+03	0.53329E-06	0.19428E+01
YES		NO	CONT	0.41251E+02	0.34000E+02	0.22050E+07	0.43656E+02	0.14560E+02	0.00000E+00
0.00000E+00		0.23445E+02		0.36550E+03	0.16792E+08	0.00000E+00	0.00000E+00	0.88809E-02	0.12796E+01
		0.10788E+05		0.14778E+02	0.34000E+02	0.78993E+06	0.16679E+02	0.17954E+05	0.20632E+05
1	4	1	PLAT	0.00000E+00	0.64000E+01	0.00000E+00	0.20531E+03	0.35788E+01	0.17442E+01
YES		NO	CONT	0.35769E+02	0.23702E+02	0.19119E+07	0.41295E+02	0.14605E+02	0.00000E+00
0.00000E+00		0.12869E+02		0.24558E+03	0.26038E+08	0.00000E+00	0.00000E+00	0.51613E-02	0.11625E+01
		0.73032E+04		0.96890E+01	0.32922E+02	0.51791E+06	0.13199E+02	0.10325E+05	0.16550E+05
1	5	1	PLAT	0.00000E+00	0.12800E+02	0.00000E+00	0.21061E+03	0.71577E+01	0.13318E+01
YES		NO	CONT	0.26757E+02	0.33424E+02	0.14302E+07	0.33368E+02	0.14656E+02	0.00000E+00
0.00000E+00		0.60972E+01		0.12638E+03	0.32626E+08	0.00000E+00	0.00000E+00	0.24960E-02	0.97644E+00
		0.34673E+04		0.39277E+01	0.31463E+02	0.20995E+06	0.76923E+01	0.31584E+04	0.10128E+05

treats the energy and momentum exchange between the gas and particles. Since the regions of interest on the Space Shuttle launch complex are dominated by the impingement of the viscous portions of the exhaust plumes, it was necessary to perform a plume mixing calculation and superimpose these results on the inviscid RAMP results.

The model chosen to perform the mixing calculation was the LAMP code [9] which is similar to the LAPP code [16]. The LAMP code is a forward marching finite difference code which solves the boundary layer form of the governing equations. Necessary input to the code is a set of initial jet and free-stream conditions (pressure, temperature, velocity, Prandtl number, Lewis number, and species distributions) as well as an eddy viscosity or Turbulent Kinetic Energy (TKE) model to relate the turbulent shear stress to a viscosity. The selection of an appropriate set of initial conditions as well as the use of a proper eddy viscosity or TKE model has been the subject of an enormous amount of study by numerous investigators over the past several years.

The initial conditions used for the mixing calculations were obtained by averaging the exit plane gas properties as calculated by RAMP and expanding or compressing them to atmospheric conditions using the method of Sukanek [27]. A jet radius was then calculated so as to get the same mass flow as the rocket motor. It should be noted that all gas species except aluminum containing species are used to generate the startline. The mass flow rate used to determine the jet size is the total flow rate of the motor including the Al_2O_3.

The turbulent shear stress model used for these calculations was the 2-equation TKE model of Launder et al. [17]. This model was chosen based on previous work presented in Ref. [13] which used this TKE model to compare with model engine data similar in Mach number and density ratio to the SRM sea level plume. One of the drawbacks of a TKE model is the necessity to specify initial distributions of kinetic energy and dissipation rate. The initial kinetic energy is a function of the turbulent velocity fluctuations, and the dissipation rate is related to the kinetic energy via a turbulent length scale. To obtain the results of Ref. [13], a parametric study was performed using the TKE model, the LAMP code, and a data base of model rocket plume pitot pressure data to determine a general set of initial length scales and turbulent fluctuations. This study recommended a 5 percent velocity fluctuation at the jet edge, a 0.5 percent fluctuation in the remainder of the core and a 0.1 percent velocity fluctuation in the ambient air. The initial turbulent scale length was 2.5 percent of the nozzle exit radius.

An application [22] of the plume analysis technique is shown in Fig. 13. The data consist of an impingement pressure distribution which results from an 8.5 in. exit diameter solid motor impinging on a flat plate 12.2 and 17 ft from the exit. As can be seen, the comparison is quite good.

For these calculations, the particles were assumed to be in thermal and dynamic equilibrium with the viscous plume. This assumption is probably adequate, leaving the question as to how the particle cloud disperses in the viscous plume. Calculations were made in which particulate mass was first eliminated from the viscous calculations, then the particulate momentum flux was calculated at a particular station of interest, while making the assumptions of either no dispersion or complete dispersion. The results of

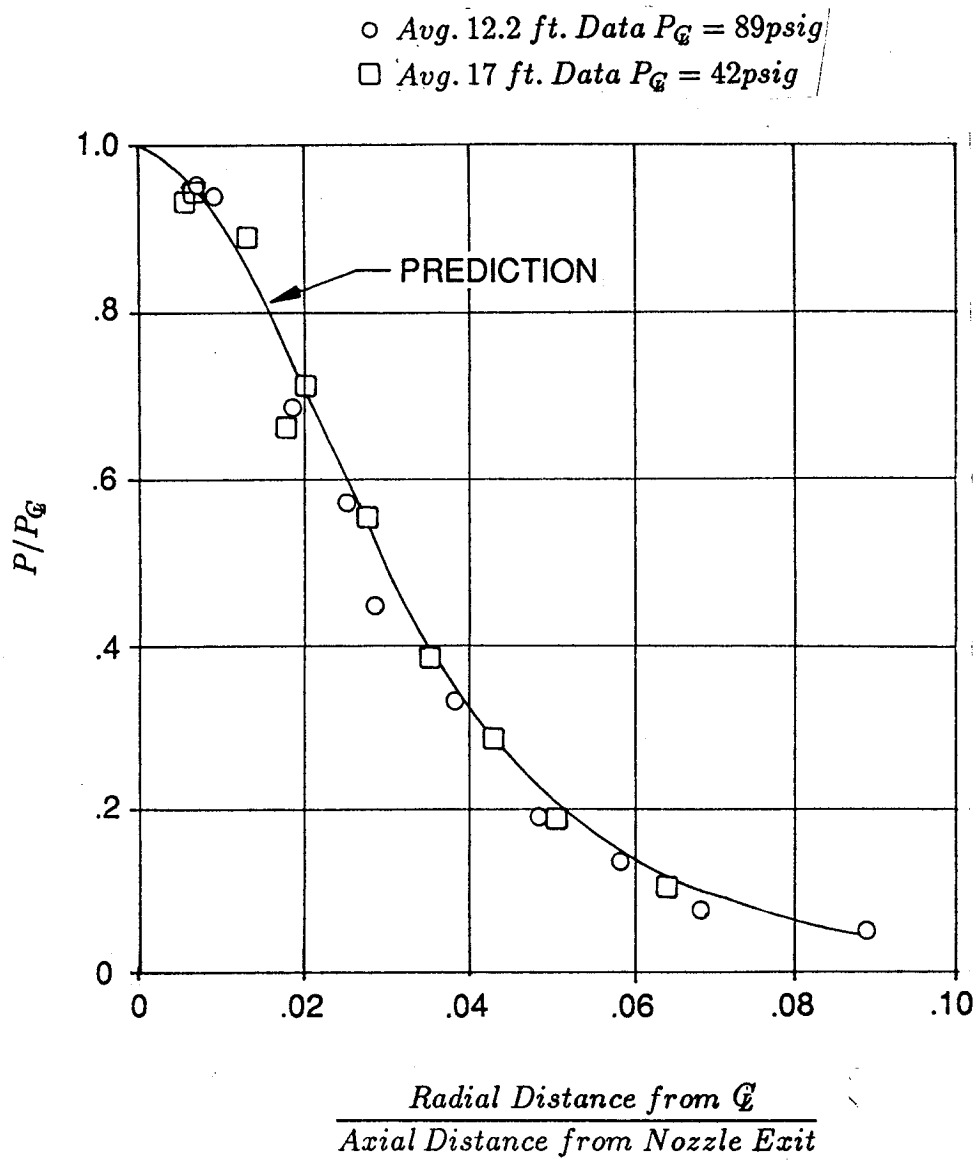

Figure 13: Comparison of 12.2 Ft Data and 17 Ft Data

these calculations did not result in as good an overall prediction as did the previously mentioned technique. Inherent in this plume model is the assumption that the particles transfer most of their momentum to the gas before they impinge on the body of interest. For large bodies relative to the plume (MLP deck), the experimental results of Ref. [26] support this assumption. For small bodies relative to the plume, this assumption is probably not as valid, but the resulting forces on the body are probably close to the results which are predicted using the plume model presented here.

The results presented here are for the fully viscous plumes since the area of interest in the SRM plume was downstream of the point where the shear layer penetrated to the centerline. Therefore, the flow properties of the SRM plume which are shown in Figs.14 through 18 present only the viscous flow characteristics. A description of the inviscid plume can be found in Ref. [28].

Figure 14 presents the radial distribution of Mach number at various axial stations in the plume. Figure 15 gives radial distribution of pitot total pressure. Figure 16 shows the radial distributions of the gas recovery temperature. Figures 17 and 18 show the particle properties of the plume. Figure 17 shows the radial distributions of particle mass flux while Fig. 18 gives the radial distribution of particle total energy (kinetic + thermal) flux.

A limited amount of experimental [26,29] heat transfer data was available which could be used to determine an accommodation coefficient which could be used for thermal environment predictions for the MLP. Plumes were developed for the Titan and Tomahawk motors for which the data was available, but no single accommodation coefficient could be determined which would correlate the experimental data, even though the particulate mass fluxes at the regions of interest in the two plumes were approximately the same. These results led to investigations of possible impingement flowfield or shock layer effects which might supply an adequate correlation.

4.4.2 Impingement Flowfield

The standard method of calculating particle impingement heating to a body immersed in a two-phase plume is to consider that the particles pass through the shock layer experiencing no change in the kinetic or thermal energies. The difference in observed heating rate and incident particle total energy is then accounted for by means of an accommodation coefficient. This method is probably adequate for very small bodies relative to the plume diameter and at high altitudes where the shock is relatively close to the impinged surface. At low altitudes (low Mach number) and cases where large bodies are impinged by small plumes the shock ahead of the body may stand off the body at significant distances. In this case, as the particles travel through the shock layer they can be influenced by the relatively dense gas. As a result, the particles can be turned as well as heated and decelerated.

To more adequately determine the mass and energy fluxes of the particles that can actually strike a body (such as the MLP deck) in the SRM plume, particle streamlines were traced through the shock layer ahead of an impinged body. A parametric analysis of the particle trajectories behind the shock were performed for the plumes through

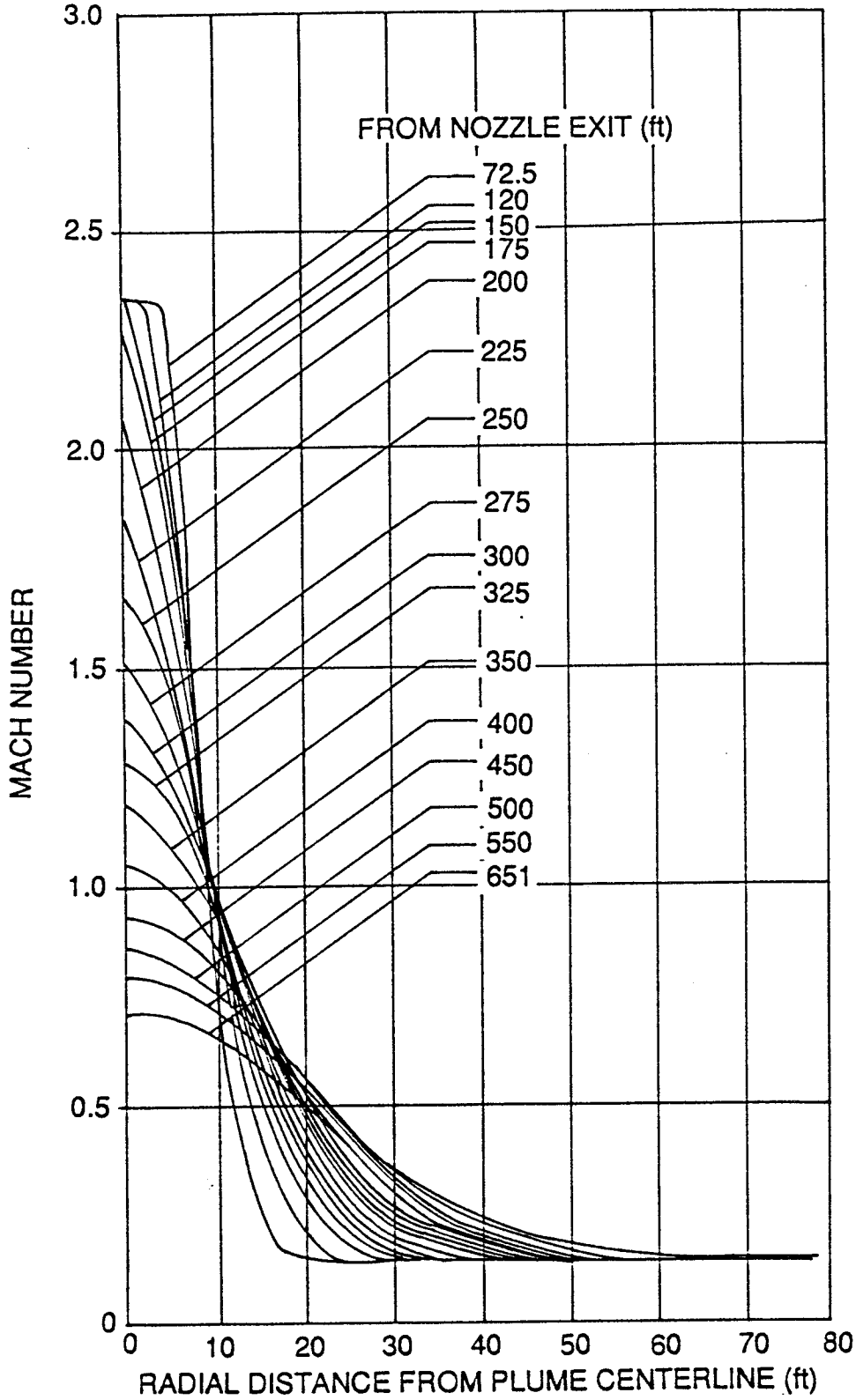

Figure 14: Space Shuttle SRM Radial Distributions of Mach Number

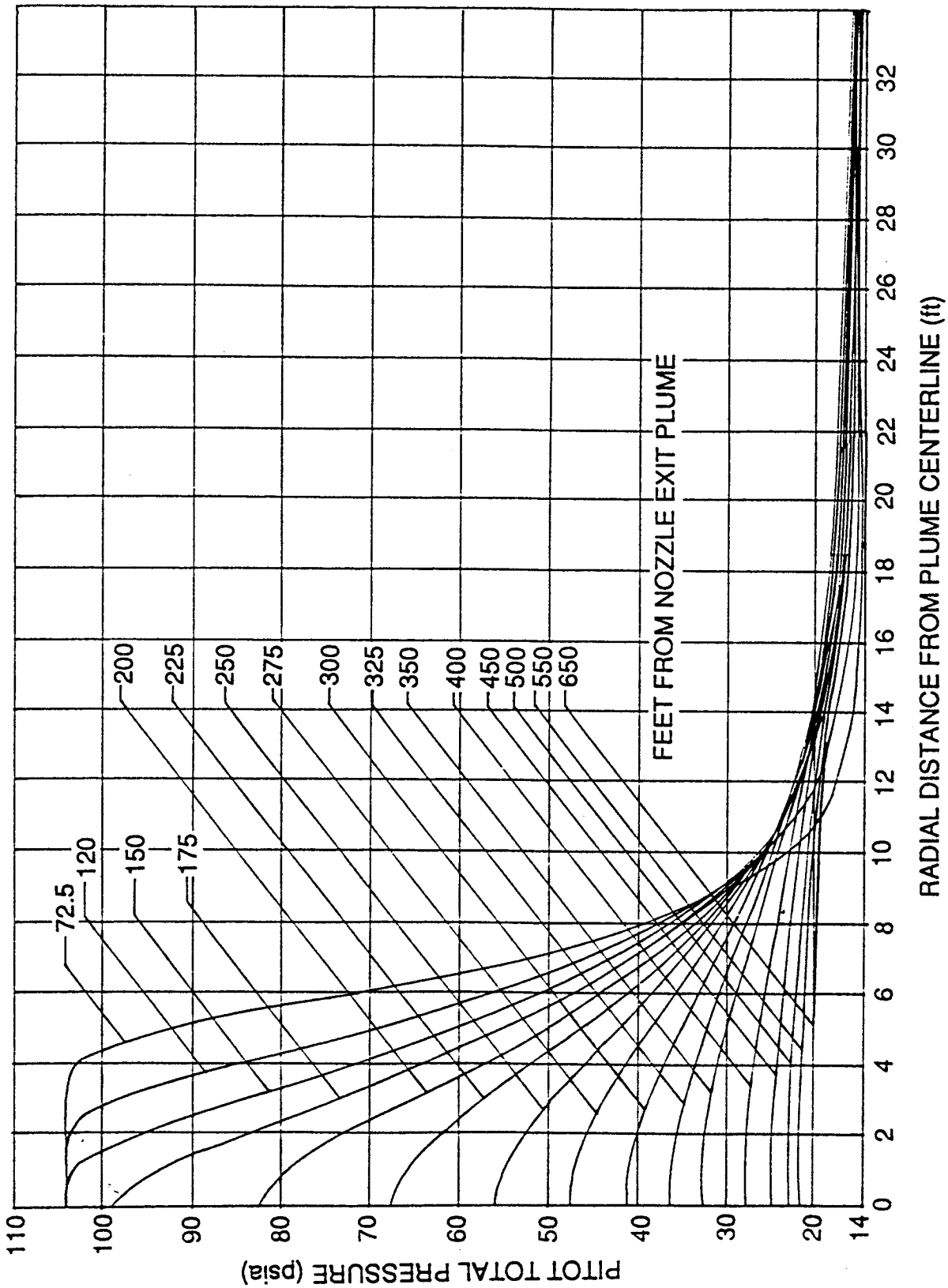

Figure 15: Sea Level Space Shuttle SRM Radial Pitot Total Pressure Distribution

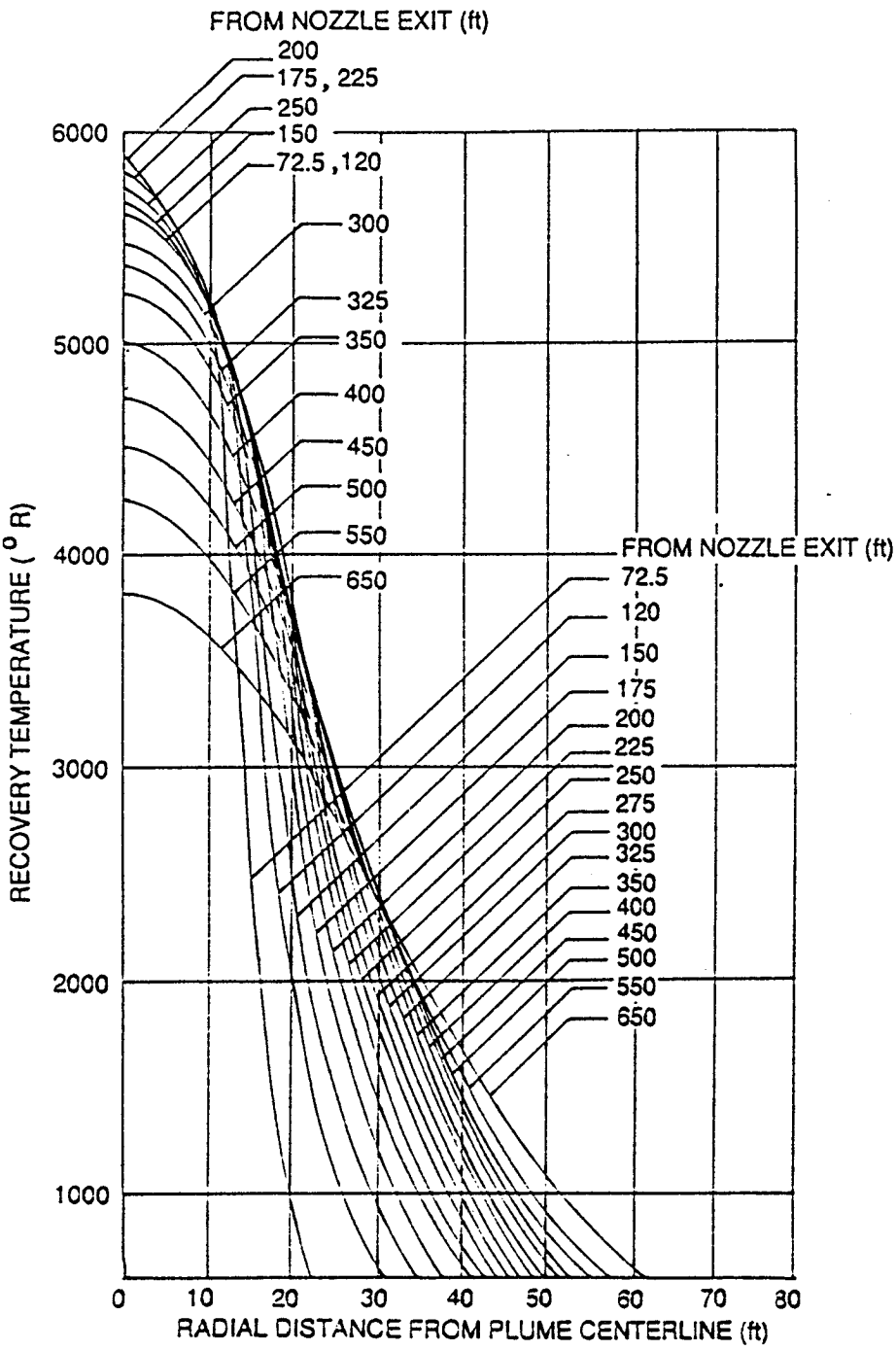

Figure 16: Space Shuttle SRM Radial Gas Recovery Temperature Distributions

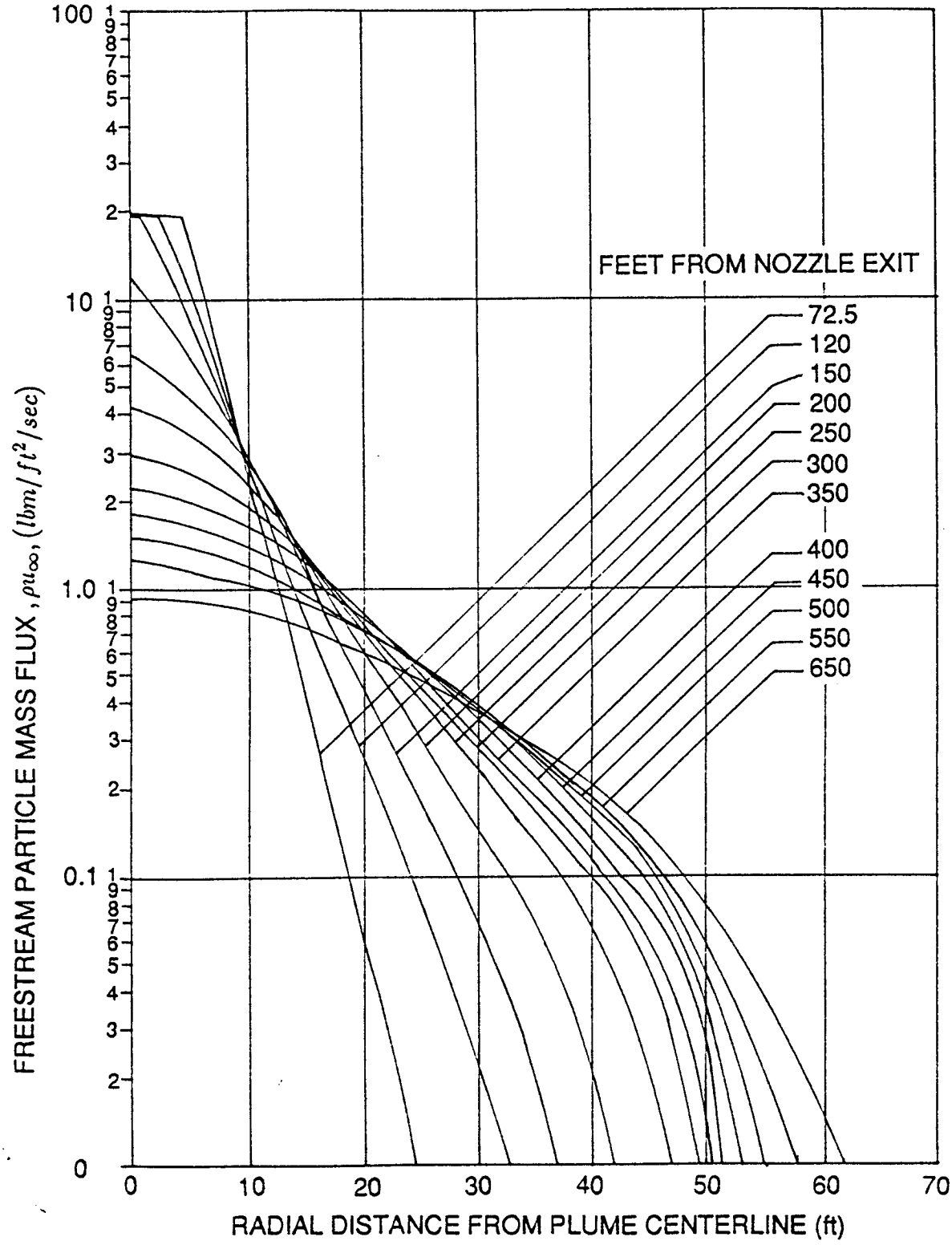

Figure 17: Space Shuttle SRM Radial Distributions of Undisturbed Plume Particle Mass Flux

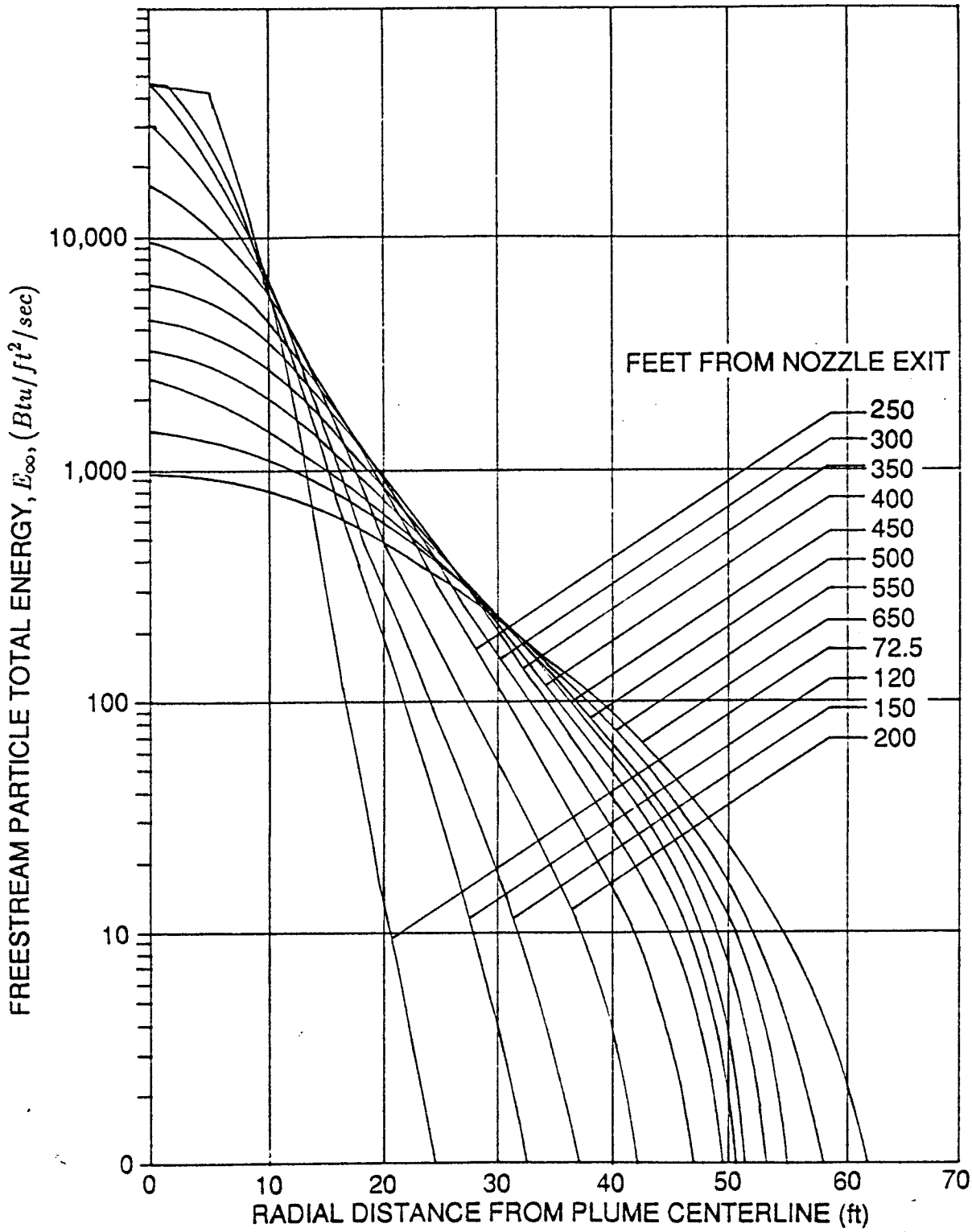

Figure 18: Space Shuttle SRM Radial Distributions of Undisturbed Plume Particle Total Energy

variations in Mach number and effective body radius of curvature. Effective radius of curvature is the radius of curvature of a sphere that has the same velocity distribution as the body of interest. The shock standoff distance and velocity distribution behind the shock were determined using the method of Truitt [30]. Once the shock layer properties were established, particles of the same size as the SRM plume were tracked through to the wall and the actual mass and energy fluxes at the surface were calculated. The results of these calculations are presented in Figs. 19 and 20. Figure 19 presents the ratio of the particle mass flux at the surface to the upstream mass flux (Fig. 17) as a function of local plume Mach number and body effective radius of curvature. Figure 20 presents the ratio of particle total energy at the impinged surface to the free-stream total energy (Fig. 18) as a function of local plume Mach number and body radius of curvature. The effective radius of curvature of an infinite flat plate (MLP deck) located at various distances from the SRM exit plane are given in Fig. 21. For other arbitrary geometries the method presented in Ref. [31] can be used. If the body uses a sphere or a cylinder then the actual radius of curvature may be used.

4.4.3 Convective Heating Rates

The gaseous convective heating rates are contributors to the overall thermal environment produced by solid rocket exhaust plume impingement. Since the SRM plume impingement problem of interest involves predominantly stagnation type heating, a simplified approach to calculating the convective heating environment was adopted for the overall model.

Stagnation point heating rates for a 1 ft sphere were calculated at various points down the centerline of the SRM plume. These calculations were made using the method of Marvin and Diewert [32] and the computer code of Ref. [33]. Additionally, the viscous plume is highly turbulent. Previous investigators [34] have shown that turbulence in the exhaust plume amplifies the heating rate one would normally predict. Reference [34] has a correlation of amplification factor as a function of local Eckert number and mean velocity fluctuation. Amplification factors were calculated for the SRM plume and applied to the stagnation point heating rates previously calculated. The resultant centerline distribution of stagnation point heating rates for the SRM plume are shown in Fig. 22.

The primary application of the SRM plume was to predict the thermal environment to the MLP deck (a large body relative to the plume). To account for variations in total pressure and temperature of the centerline of the plume, Fig. 23 was generated. This figure presents local/centerline heating rate ratios at various axial stations in the SRM plume. The use of Figs. 22 and 23 allows the designer to determine a convective heating rate at any point in the plume, assuming that the plume is impinging on an infinite flat plate.

It is possible to use the data presented in Figs. 22 and 23 for small bodies which are impinged on by the SRM plume. To obtain a local/centerline heating rate ratio for a small body use the following equation:

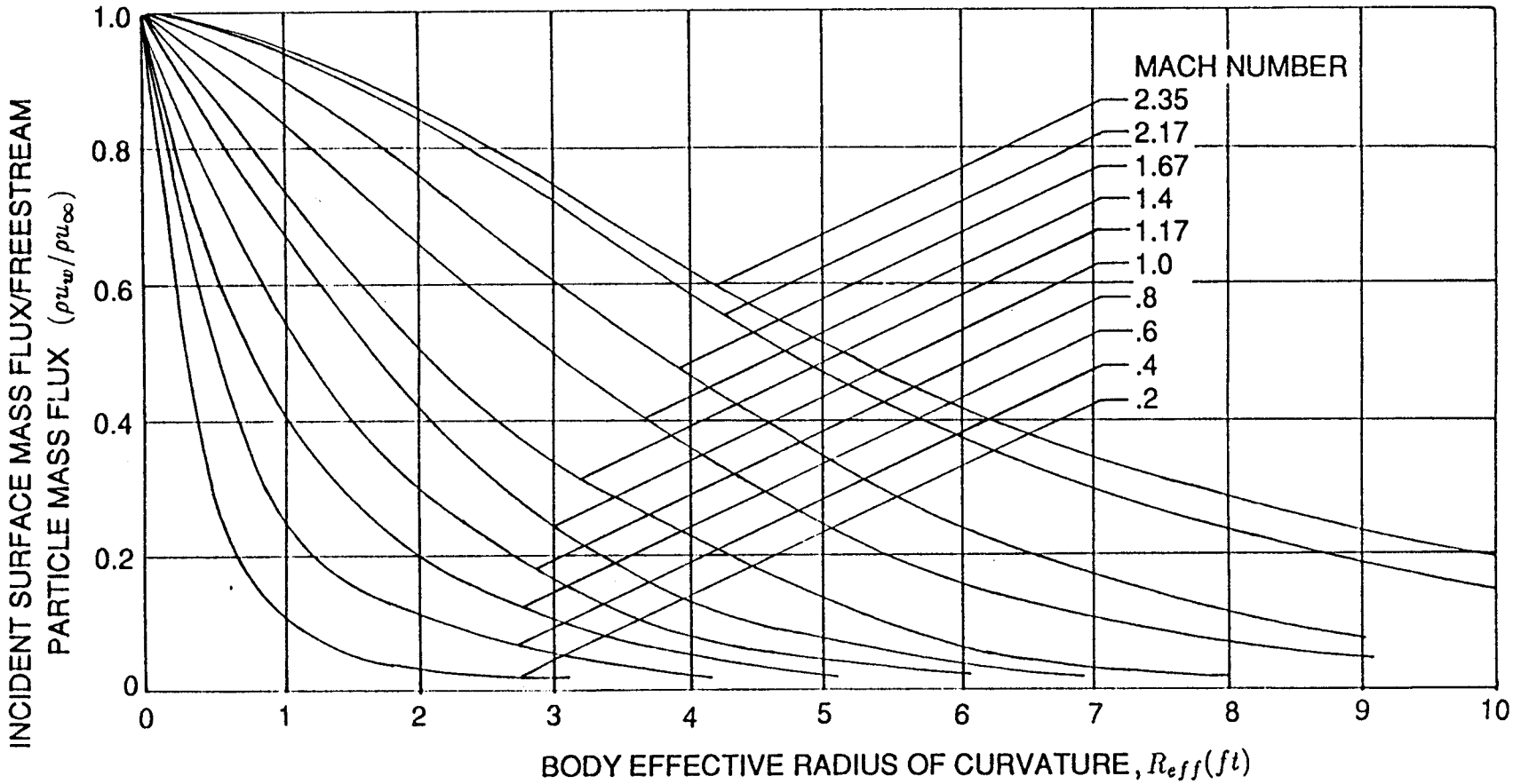

Figure 19: Space Shuttle SRM Ratio of Incident Particle Mass Flux to Undisturbed Plume Particle Mass Flux as a Function of Local Plume Mach Number and Impinged Body Effective Radius of Curvature

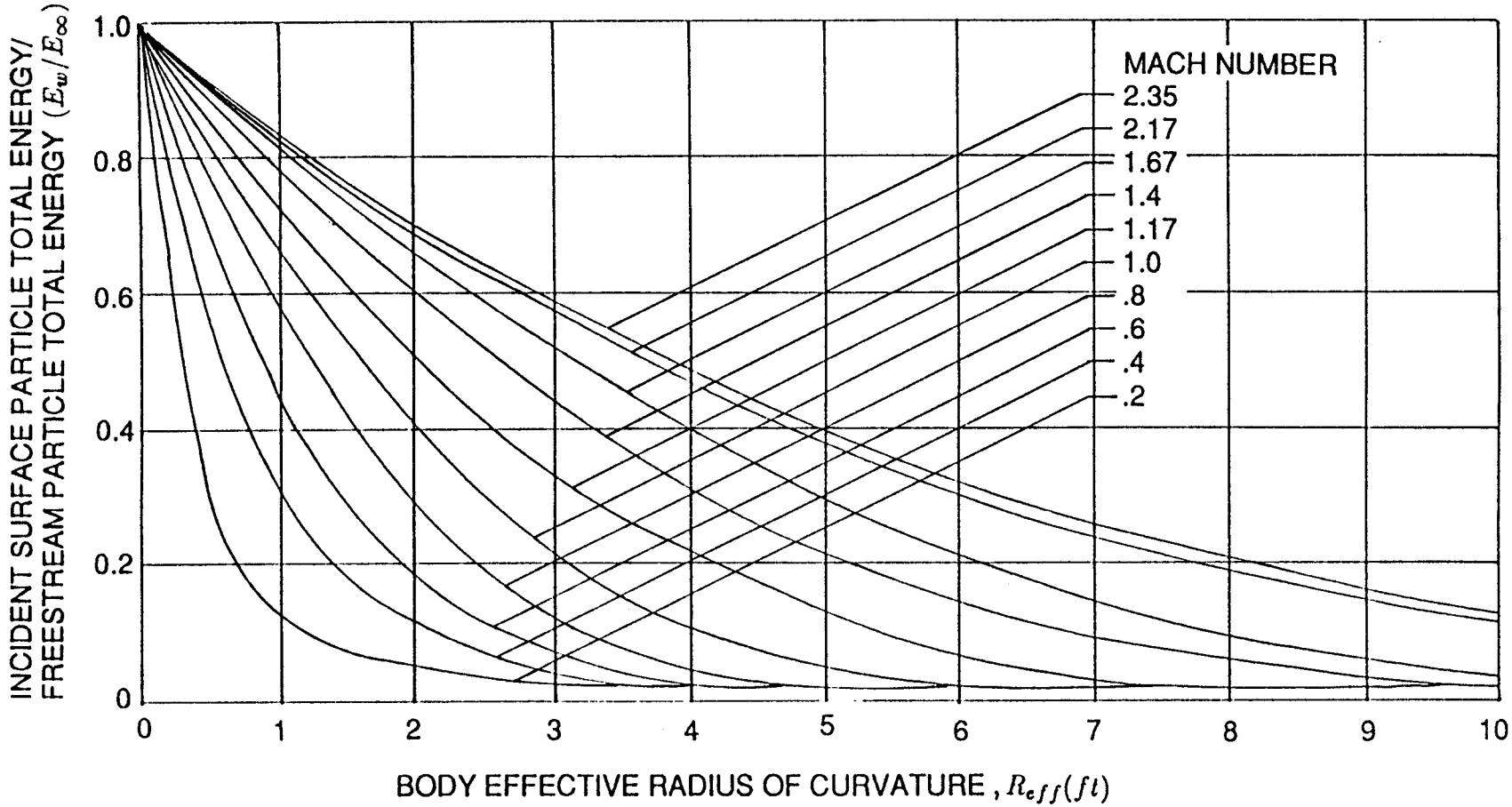

Figure 20: Space Shuttle SRM Ratio of Incident Particle Total Energy Flux to Undisturbed Plume Particle Total Energy Flux as a Function of Local Plume Mach Number and Impinged Body Effective Radius of Curvature

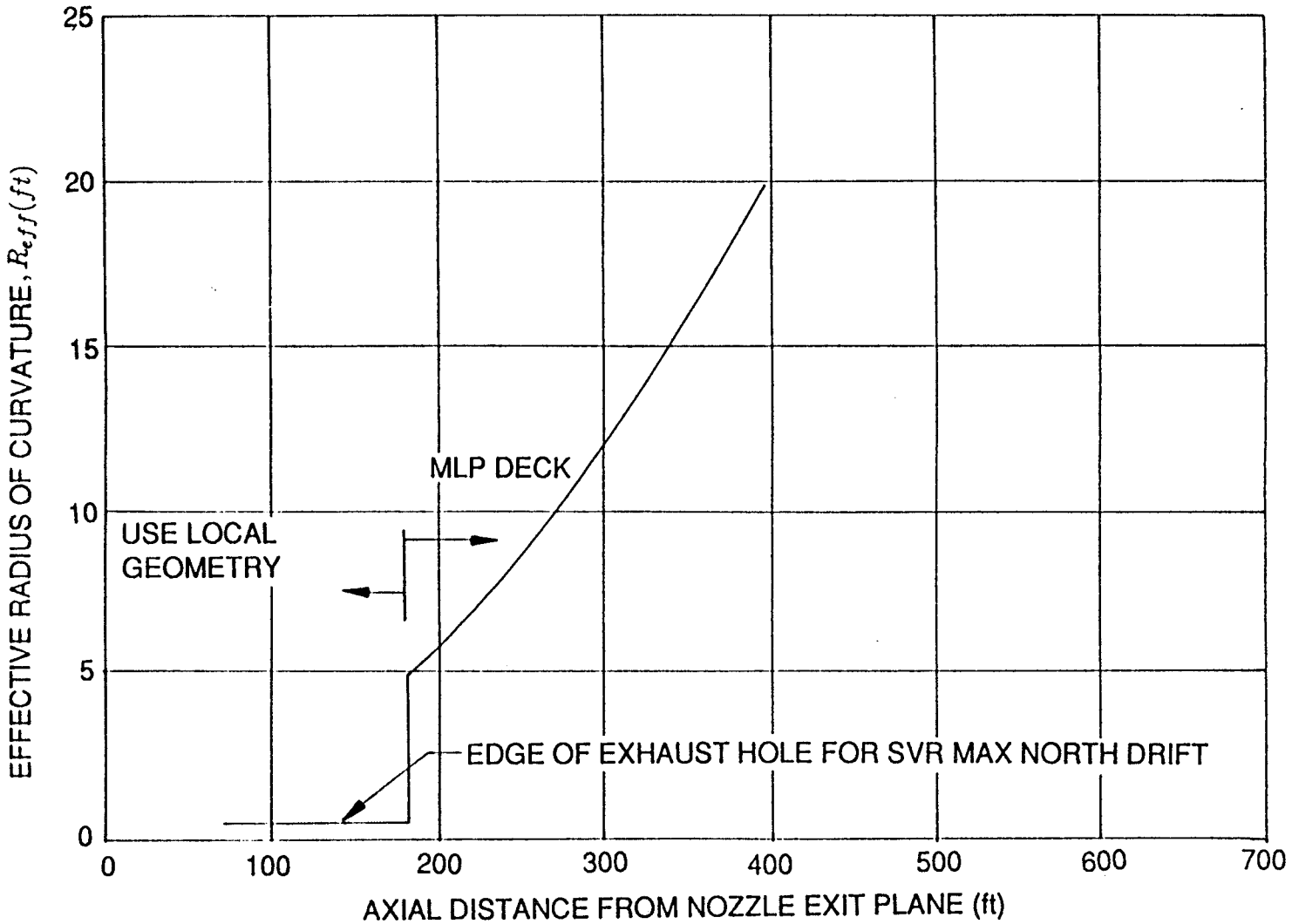

Figure 21: Effective Radius of Curvature of an Infinite Flat Plate Impinged upon by the Space Shuttle SRM

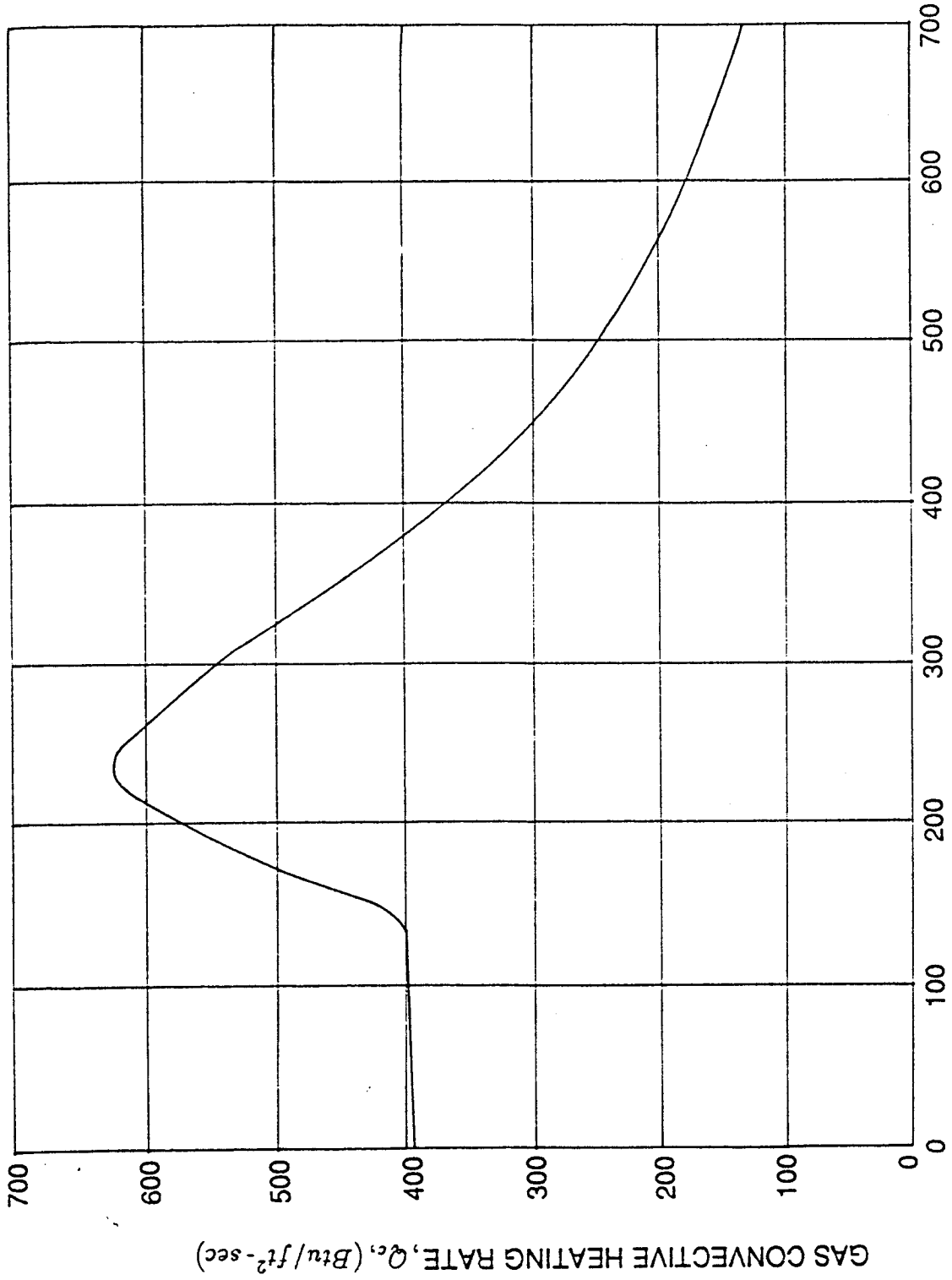

Figure 22: Space Shuttle SRM Centerline Stagnation Point Convective Heating Rate on a 1 Ft Sphere at 300 K Wall Temperature

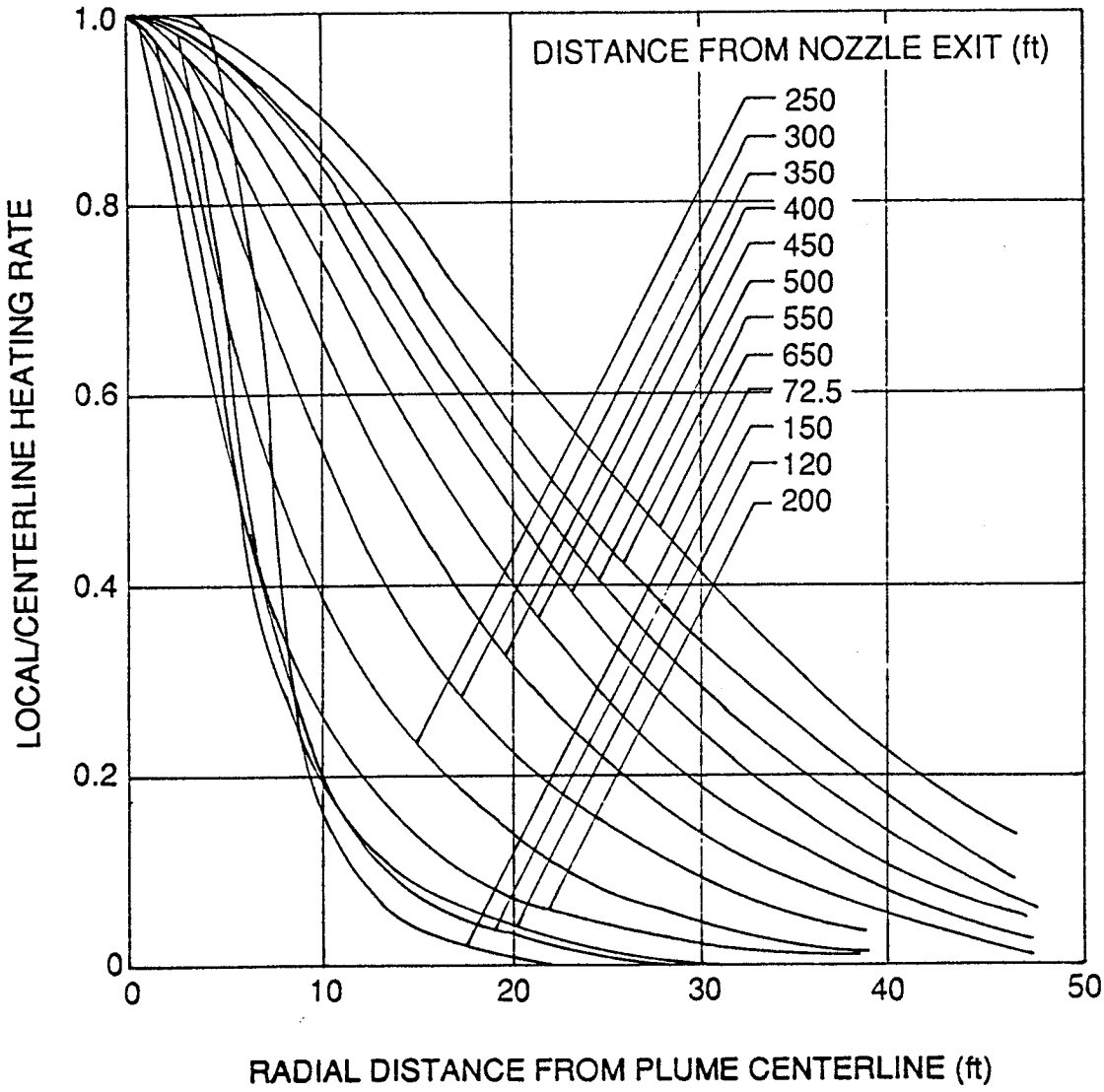

Figure 23: Space Shuttle SRM Local-to-Centerline Convective Heating Rate Ratio

$$q/q_{cl\ (small\ body)} = (q_e/q_{cl})_{(Fig.\ 23)} \times (P_{cl}/P_l)^{.5}$$

where P_{cl} is the centerline impingement pressure and P_l is the local plume impingement pressure. This equation accounts for the fact that for a large body the local heating rate is a function of the local impingement pressure/stagnation impingement pressure to the 0.9 power, while for small bodies the off centerline/centerline stagnation heating rate ratio is a function of stagnation pressure ratios to the 0.5 power. Once the stagnation point heating rate has been determined to a 1 ft radius sphere, the heating rate must be corrected for the actual effective radius of curvature. The effective body radius of curvature for a sphere is the actual body radius, but the calculation of the radius of curvature for arbitrary bodies is somewhat more complicated. Reference [31] has a detailed discussion of the determination of the effective radius of curvature of the MLP deck at various locations in the SRM plume. These results were previously shown in Fig. 21. Once the effective radius of curvature is determined, divide the 1 ft sphere stagnation heating rate by the square root of the effective body radius of curvature to determine the actual heating rate.

4.4.4 Thermal Model

The data which have been previously described are sufficient to calculate the thermal response of a structure immersed in the SRM plume except for an accommodation coefficient that specifies what portion of the particle total energy that exists at the surface is actually transferred to the surface as a heating rate.

Recently, there were some measurements taken during a Titan IIIC launch [29] and some observed melting of a steel plate during the Tomahawk impingement test [26]. The Titan IIIC data consisted of some measured heating rates along with the qualitative results that the surface did come fairly close to melting. The Tomahawk data consisted of pressure data at 12 and 17 ft from the motor exit and observed melting through a 1 in. plate at 12.2 ft and 3/4 in. melting at 17 ft.

In order to use this type of data, it was necessary to utilize a thermal analyzer that would take the surface heating rate time history as calculated using the previously mentioned model and determine the time history temperature and natural responses of the impinged surfaces. The thermal analyzer which was utilized is described in Refs. [35,36].

By using the same methodology for the Titan IIIC and Tomahawk plumes and calculating the thermal response of the bare steel of the Titan IIIC box and Tomahawk plate, it was not possible to match the two sets of data. Figure 24 shows the results of these calculations. For the Tomahawk data, a 3/4 in. melt depth of the steel requires an accommodation coefficient of approximately 0.34. Applying the same coefficient to the Titan plume would predict approximately 1/8 in. of the box melting which was not observed after the test. Based on these calculations and because significant amounts of Al_2O_3 coating were observed on the Titan box and Tomahawk plate at the end of the

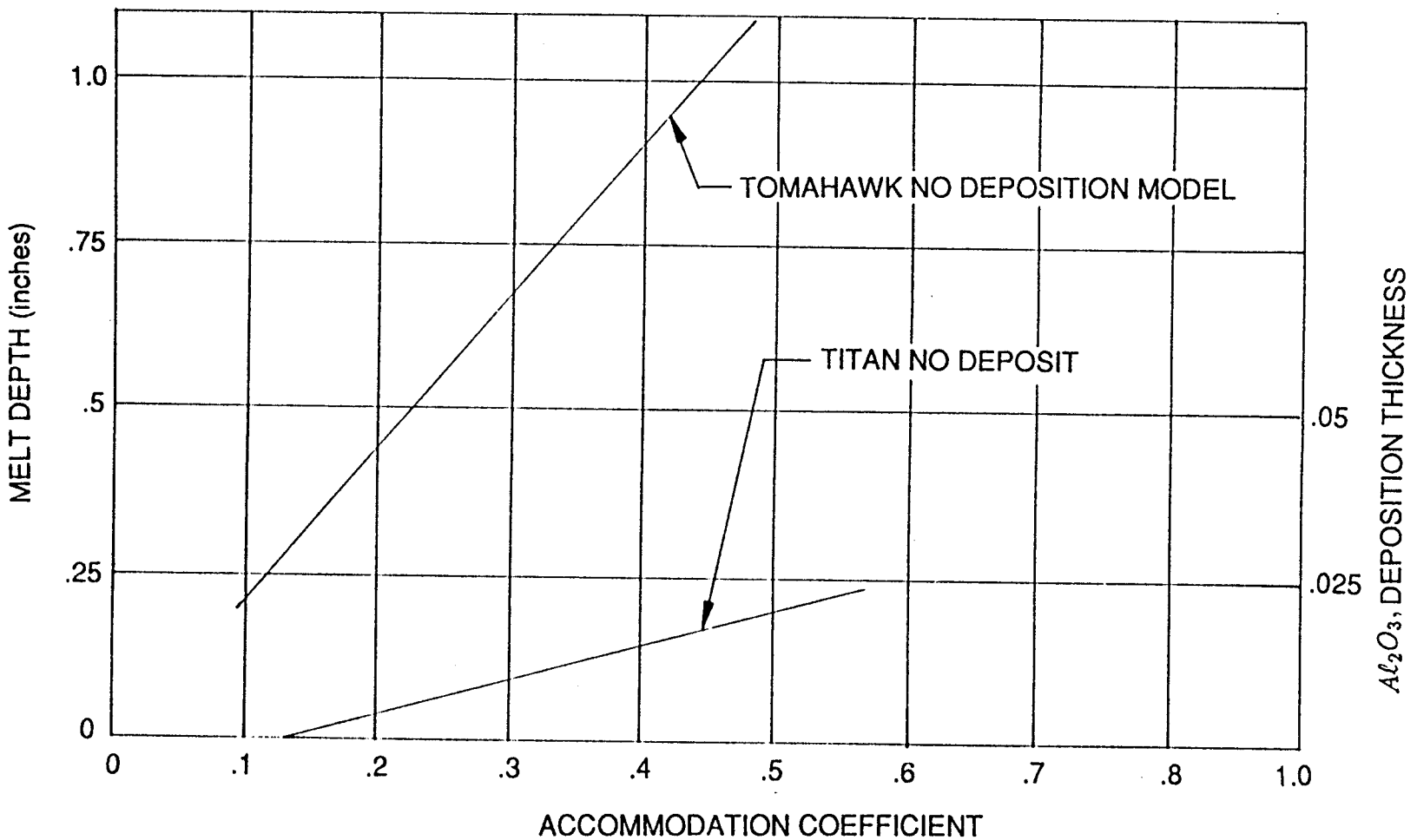

Figure 24: Titan Box II and Tomahawk 17–Ft Melt Thickness and Aluminum Oxide Layer Thickness as a Function of Particle Surface Accommodation Coefficient

firing, it was decided to investigate an Al_2O_3 deposition model to see if a coating might possibly correlate the two pieces of data and allow a single accommodation coefficient that would match the data.

The resulting thermal model used the time history of gas recovery temperature, cold wall convective heating rate, particle mass and energy fluxes at the surface and an assumed accommodation coefficient as input conditions. The model starts off with cold steel and keeps track of how much Al_2O_3 is deposited on the surface until enough has been added to build up a 0.002 in. layer at which point a node is added. The mass is added to the surface via the following:

$$\Delta = (\alpha/\rho_{A1203}) \int_{t}^{t+dt} (\rho V)_w dt$$

where Δ is the incremental Al_2O_3 thickness, α is the accommodation coefficient, ρAl_2O_3 is the specific density of Al_2O_3 and $(\rho v)_w$ is the mass flux at the surface. Mass continues to build up on the surface in 0.002 in. layers until the surface temperature of the Al_2O_3 reaches melt temperature of 4170°R. Heat is added to the surface at the surface temperature by the following:

$$Q_{HW} = Q_{c,CW*}((T_{oR} - T_{wall})/(T_{oR} - 540)) + \alpha\,(\rho v)_w\,(H_p - H_w)$$

where Q_{HW} is the actual heating rate to the surface at the surface temperature, $Q_{c,CW*}$ is the input cold wall heating rate, T_{oR} is the gas recovery temperature, T_{Wall} is the surface temperature, H_p is the particle enthalpy at the surface which is determined by dividing the particle total energy at the wall by the particle mass flux at the wall, and H_W is the enthalpy of aluminum oxide evaluated at the surface temperature. Once the surface has heated up to 4170°R, heat continues to be added and the Al_2O_3 is allowed to absorb the heat of fusion and then super heat. This process continues until enough heat has been conducted through the Al_2O_3 layer to the first steel node to elevate its temperature to the melting point. Then the steel node is allowed to absorb its heat of fusion. Once this occurs the steel node and the entire Al_2O_3 deposition layer is removed and the entire deposition process continues until the plume no longer influences the surface. Many other assumptions, node sizes, etc., were made prior to finalizing the thermal model. The model which was finally chosen did the best job of correlating the limited amount of data.

When this thermal model was applied to the Titan IIIC and Tomahawk data, an accommodation coefficient of 0.55 resulted in no melting of the Titan IIIC box surface, and 3/4 in. of steel melted for the Tomahawk case. The results of these calculations are presented in Fig. 25. This figure presents the melt thickness and Al_2O_3 deposition thickness versus accommodation coefficient. The model when applied to the Titan data predicted no melting at any accommodation coefficient. Figure 26 presents a time history of what the model predicts for the response of the Titan box

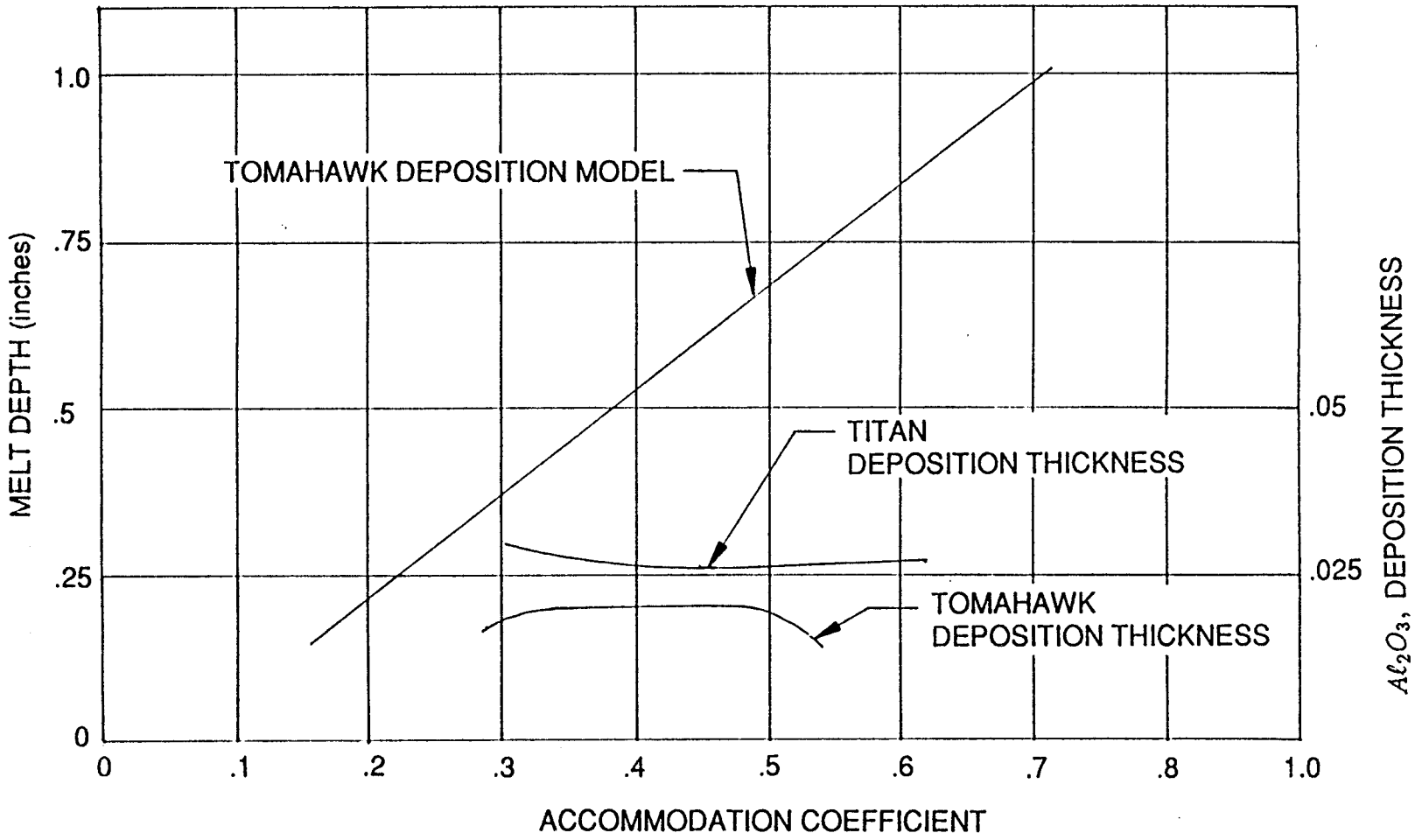

Figure 25: Titan Box II and Tomahawk 17–Ft Melt Thickness and Aluminum Oxide Layer Thickness as a Function of Particle Surface Accommodation Coefficient

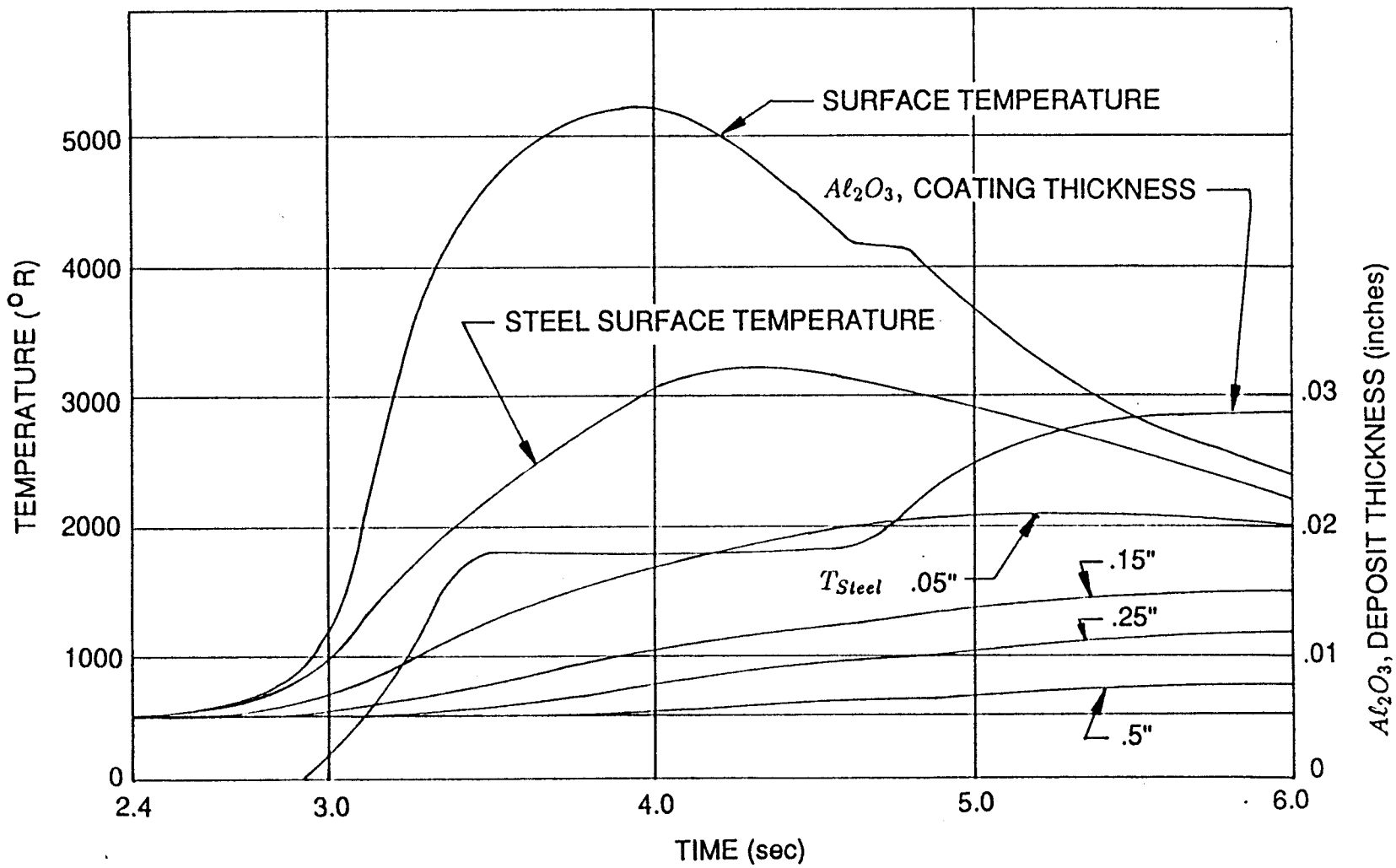

Figure 26: Titan IIIC Box 2 Thermal Analysis Results

to the plume. The Al_2O_3 surface temperature superheats to about 5200R while the steel surface barely reaches melt temperature but cannot absorb the heat of fusion and thus does not melt. Also shown on this figure is the deposition thickness time history and the temperature distribution through the steel surface. The Al_2O_3 deposition thickness which is predicted is consistent with the observed layer thickness following the test.

Probably the biggest factor in allowing the correlation of the two pieces of data was allowing a superheated molten layer of Al_2O_3 to form on the surface. Once the surface layer has absorbed the heat of fusion of the Al_2O_3 and the temperature has risen above the melt temperature the heat of fusion of the incoming Al_2O_3 energy flux cannot be added to the surface, which effectively lowers the surface heat load.

Finally, this entire model was applied to a point on the edge of the SRM exhaust hole of the MLP. It is expected that this location should be subjected to a fairly high heat load and would be indicative of the amount of deck melt that might be expected. The results of these calculations are shown in Fig. 27. This figure indicates that the steel surface reaches the melt temperature but does not absorb enough heat to melt. There is probably some slight surface melting. Also shown on this figure is the temperature-time history at different depths in the plate.

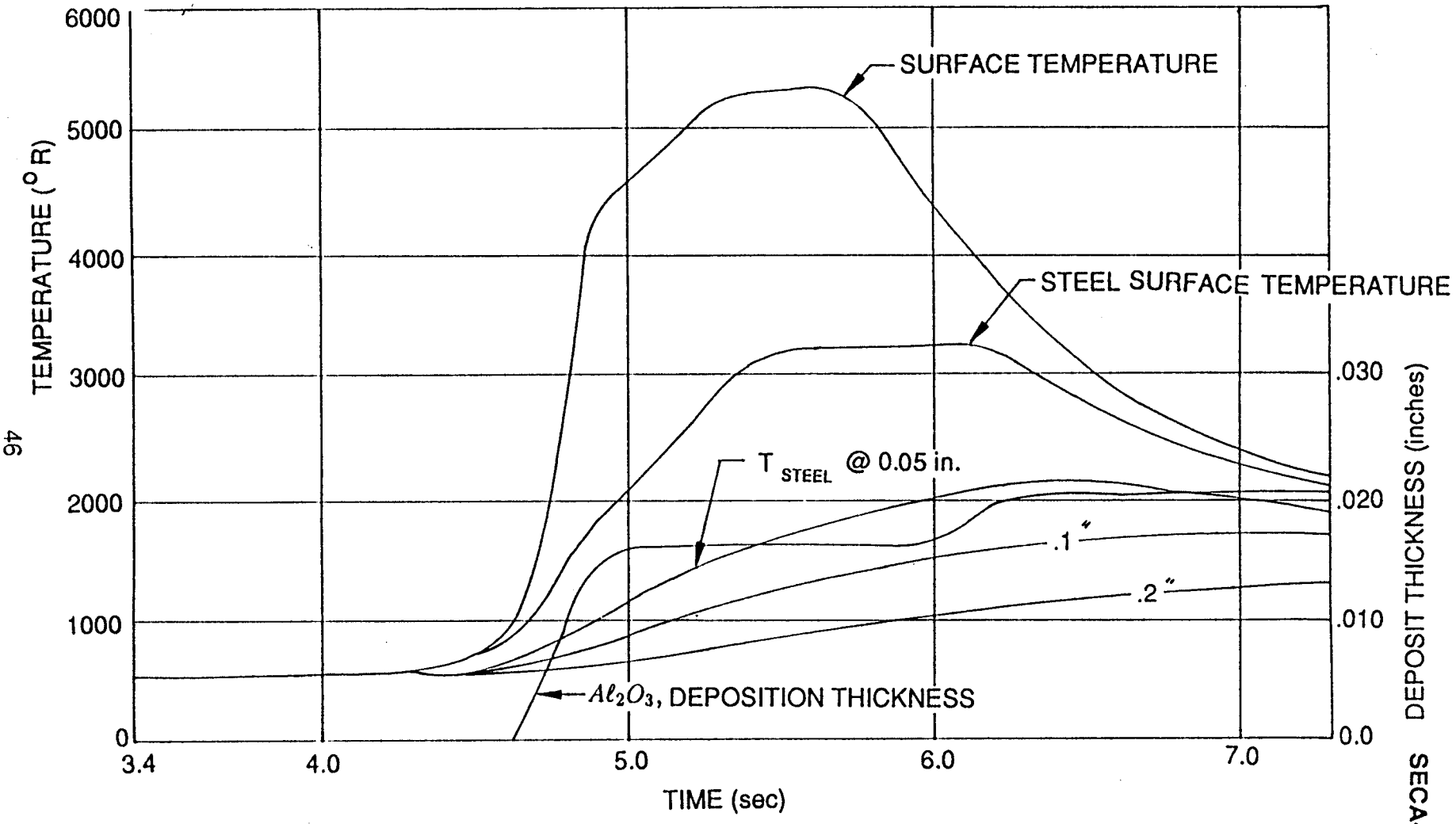

Figure 27: Results of Thermal Analysis of Edge of MLP SRM Exhaust Hole

Section 5
LEVEL III LOW ALTITUDE IMPINGEMENT ANALYSIS

The highest level of sophistication for low altitude impingement modeling would entail utilizing the more recently developed Navier-Stokes codes. These codes have the potential for modeling the entire exhaust plume including the structure that is being impinged. These codes have been extended to three dimensions so that multiple plumes can theoretically be treated although considerable validation exercises would be required. It should be noted that Level III CFD analysis are computationally fairly expensive and can require significant amounts of labor to set up the geometry and properly initialize them. CFD models would probably only be used if a Level I or II analysis could not adequately address particular problems.

An example os a Level III model is the FDNS code [10]. FDNS is a implicit Navier-Stokes solver which has several turbulence model options. It also has ideal, frozen, equilibrium and finite-rate chemistry options. Presently, under NASA funding, the code is being upgraded to treat two-phase flows. A Lagrangian particle treatment has been added and preliminary check cases have been completed. Figure 28 presents the distribution of impact pressure for the experimental data previously shown in Fig. 11. This particular case was modeled with the flat plate as a part of the solution. The calculations are within 7 percent of the measured results. These calculations included two-phase flow (22% Al), finite-rate chemistry and a two-equation turbulence model. The turbulence model is the standard model which is used by FDNS to calculate plumes and was not adjusted for this case. The solution was initiated in the combustion chamber. This is an example of the type of results that can be expected from a Navier-Stokes solver. However, these codes must be exercised against a large amount of experimental data and configurations before they can be regularly used for low altitude impingement predictions.

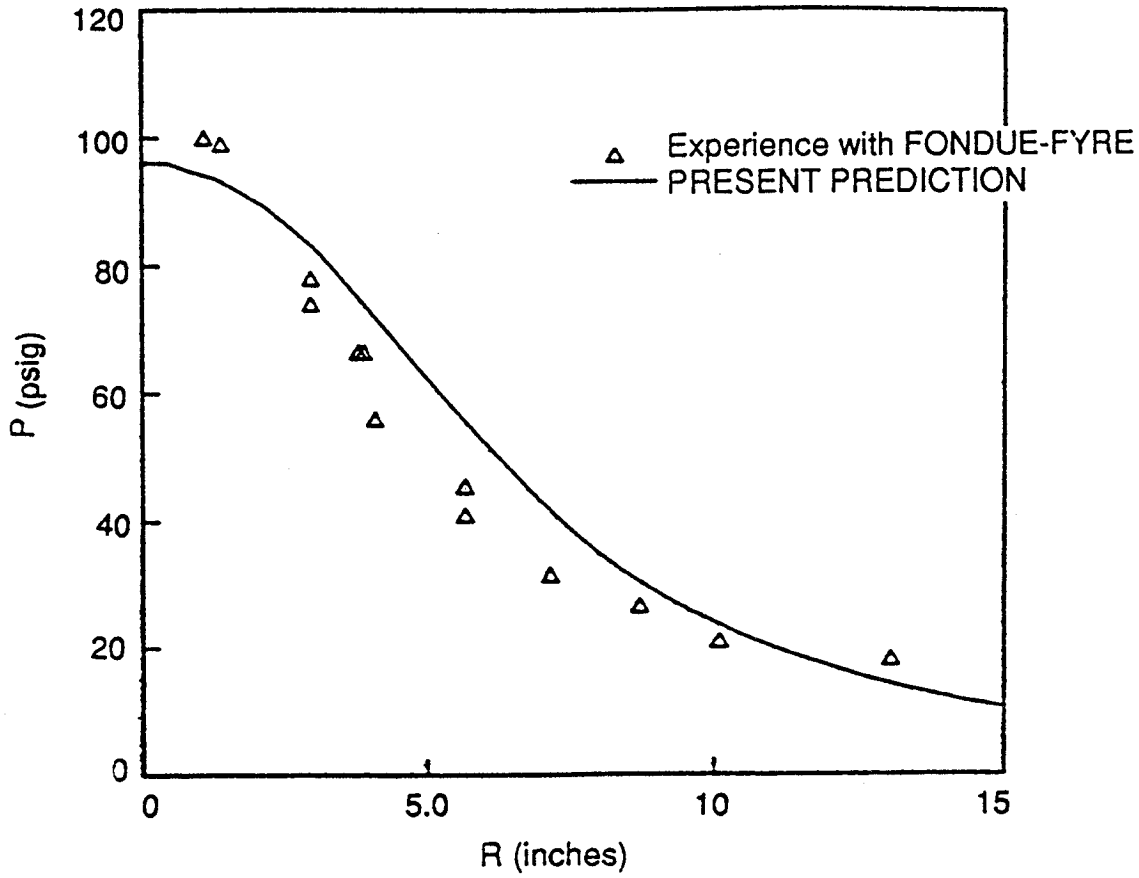

Figure 28: Tomahawk Impingement on Plate 12.2 Ft from Nozzle Exit (Five Particle Sizes Two-Phase Flow Calculation)

Section 6
REFERENCES

[1] Smith, S.D., "High Altitude Supersonic Flow of Chemically Reacting Gas-Particle Mixtures - Volume III - RAMP2 - Computer Code User's and Applications Manual," Lockheed Missiles & Space Company, Huntsville, AL, LMSC-HREC TR D867400-III, Oct. 1984.

[2] Smith, S.D., "User's Manual - Variable O/F Ratio Method of Characteristics Program for Nozzles and Plume Analysis," LMSC-HREC D162220-IV, Lockheed Missiles & Space Co., Huntsville, AL, June 1971.

[3] Doo, Y.C. and Nelson, D.A., "Direct Monte Carlo Simulation of Small Biopropellant Plumes," AFRPL TR-86-100, Aerospace Corp., Los Angeles, CA, Jan. 1987.

[4] Chirivella, J.E., "Direct Simulation Monte Carlo of Vacuum Plumes - AFE RCS Plumes," ER-SP-1016, Engo Tech Systems, Inc., Tujunga, CA, Sep. 1988.

[5] Heuser, J.E., Melfi, L.T., Bird, G.A., and Brock, F.J., "Analysis of Large Solid Propellant Rocket Engine Exhaust Plumes Using the Direct Simulation Monte Carlo Method," AIAA-4-0496, paper presented at the AIAA 22nd Aerospace Sciences Meeting, Reno, Nevada, Jan. 1984.

[6] Piesik, E.T. and Roberts, D.J., "A Method to Define Low-Altitude Rocket Exhaust Characteristics and Impingement Effects," *J. of Spacecraft and Rockets*, 7, April 1970, pp. 446-451.

[7] Piesik, E.T., "Aluminized Propellants and a Method Defining Low-Altitude Exhaust Plumes", *J. of Spacecraft and Rockets*, Vol. 23, No. 2, March-April 1986, pp. 215-221.

[8] Dash, S.M., Pergament, H.S., and Thorpe, R.D, "A Modular Approach for the Coupling of Viscous and Inviscid Processes in Exhaust Plume Flows", 17th Aerospace Sciences Meeting, New Orleans, Jan. 1979.

[9] Ratliff, A.W. et al., "Chemical Laser Analysis Development; Vol. 1, Laser and Mixing Program and User's Guide," Lockheed Missiles & Space Company, Huntsville, AL, Oct. 1973.

[10] Chen, Y.S., "Compressible and Incompressible Flow Computations with a Pressure Based Method," AIAA-89-0286, 27th Aerospace Sciences Meeting.

[11] Anon., "Saturn V Launch Complex Plume Induced Pressure and Thermal Environment," The Boeing Co.

[12] Will, C.F., "Thermal Environment Computer Program for Solid Rocket Exhaust Analysis," TN-AP-69-419, Chrysler Space Division, June 1990.

[13] Smith, S.D., "Revised Predictions of the SRB Plume Impingement Pressures on the MLP (LC39) During Lift-Off," LMSC-HREC TR D568286, Lockheed Missiles & Space Co., Huntsville, AL, April 1978.

[14] Environment and Test Specification Levels Ground Support Equipment for Space Shuttle System Launch Complex 39. Vol. 11 of 11, Thermal and Pressure Part 2

of 2, Specific Temperatures of Selected Parts of LC39 GP 1059 Kennedy Space Center, FL, July 1977.

[15] Penny, M.M., Smith, S.D., et al., "Supersonic Flow of Chemically Reacting Gas-Particle Mixtures," LMSC-HREC TR D496555-II/II, Lockheed Missiles & Space Company, Huntsville, AL, Jan. 1976.

[16] Mikatarian, R.M., et al., "A Fast Computer Program for Non Equilibrium Rocket Plume Predictions," AFRPL-TR-72-94 Aerochem Research Labs, Princeton, NJ, Aug. 1972.

[17] Launder, B.E., Morse, A., Rodi, W., and Spalding, D.B., "The Prediction of Free Shear Flows. Presented at Langley Working Conference on Free Turbulent Shear Flows," NASA-Langley Research Center, Hampton, VA, July 1972.

[18] Smith, S.D., "Definition of the Viscous Sea Level Space Shuttle Solid Rocket Motor (SRM) Exhaust Plume, Impingement Flowfield and Thermal Properties Necessary to Perform a Thermal Response Analysis of the LC39 MLP," LMSC-HREC TN D697736, Lockheed Missiles & Space Co., Huntsville, AL, Nov. 1979.

[19] Tevepaugh, J.A., Smith, S.D., and Penny, M.M., "Assessment of Analytical Techniques for Predicting Solid Propellant Exhaust Plumes," AIAA Paper 77-711, AIAA 19th Fluid and Plasmadynamics Conference, Albuquerque, NM, June 1977.

[20] Fay, J.A. and Riddell, F.R. "Theory of Stagnation Point Heat Transfer in Disassociated Air," *J. of Aerospace of the Sciences*, Vol. 25, No. 2, Feb. 1958, pp. 73-85.

[21] Smith, S.D., et al., "Model Development for Exhaust Plume Effects on Launch Stand Design," SECA-89-20, SECA, Inc., Huntsville, AL, Sep. 1989.

[22] Ludwig, C.B., et al., "Standardized Infrared Radiation Model (SIRRM)", Volume I, APRPL-TR-54, Aug. 1981.

[23] Walker, J., et al., "Handbook of the Standardized Infrared Radiation Model (SIRRM)," Volume II, AFRPL-TR-81-61, Aug. 1981.

[24] Dash, S.M., et al., "The JANNAF Standard Plume Flowfield Model (SPF/2), Vol. II - Program Users Manual," SAI/PR TR-16-11, SAIC, Princeton, NJ, May 1984.

[25] Svehla, R.A., and McBride, B.J., "FORTRAN IV Computer Program for Calculation of Thermodynamics and Transport Properties of Complex Chemical Systems," NASA TN D-7056, Jan. 1976.

[26] Seymour, D.C., Greenwood, T.F., and Smith S.D., "Plume Impingement Pressure Measurements Taken During Sea Level Firings of a Tomahawk Motor," JANNAF 11th Plume Technology Meeting, Huntsville, AL, July 1979.

[27] Sukanek, P.C., "Matched Pressure Properties of Low Altitude Plumes," *AIAA J.* 15, No. 12, Dec. 1977.

[28] Smith, S.D., "Space Shuttle Solid Rocket Motor (SRM) Exhaust Plume Definitions — Sea Level to SRB Separation," LMSC-HREC TM D496879, Lockheed Missiles and Space Company, Huntsville, AL, Aug. 1976.

[29] Test Report for Titan IIIC SRM Plume Impingement Pressure Measurements at LC40 - 13 Dec. 1978. KSC-DL-126 Planning Research Corporation, Kennedy Space Center, FL, Sep. 1979.

[30] Truitt, R.W., *Hypersonic Aerodynamics*, The Ronald Press Company, New York, 1959.

[31] Wojciechowski, C.J. and Rader, R.J., "A Method of Calculating Stagnation Region Convective Heat Transfer to Arbitrary Surfaces Immersed in the Space Shuttle Altitude Control System Plumes," LMSC-HREC D162334, Lockheed Missiles and Space Company, Huntsville, AL, May 1970.

[32] Marvin, J.C., and Diewert, G.S., "Convective Heat Transfer in Planetary Gases," NASA TR R-224, July 1965.

[33] Rader, R.J., "Input Guide for the STAG-q Computer Program," TN-241-1152, Northrop Services, Inc., Huntsville, AL, Oct. 1972.

[34] Weeks, Thomas M., "Influence of Free-Stream Turbulence on Hypersonic Stagnation Zone Heating," AFFDL-TR-67-195, Air Force Flight Dynamic Lab., Wright-Patterson Air Force Base, OH, May 1968.

[35] Pond, J.E., "A Small Thermal Analyzer Package with Simplified Input," LMSC-HREC D162533, Lockheed Missiles and Space Company, Huntsville, AL, Feb. 1971.

[36] Environment and Test Specification Levels Ground Support Equipment for Space Shuttle System Launch Complex 39. Vol 11 of 11, Thermal and Pressure Part 2 of 2, Specific Temperatures of Selected Parts of LC39 GP 1059, Kennedy Space Center, FL, July 1977.

[37] Snedeker, R. S. and Donaldson, DuP. C., "Experiments on Free and Impinging Underexpanded Jets from a Convergent Nozzle," Advanced Research Projects Agency Report 63, DDC AD 461622, Sep. 1964.

[38] Unpublished Flat Plate Rocket Exhaust Impingement Data Obtained for a 20:1 Scale F-1 Rocket Engine from Marshall Space Flight Center, Huntsville, AL.

[39] Moore, G. R. and Soo Hoo, G., "Comparison of Static Rocket Motor Plume Predictions Using the JANNAF SPF-1 Model with Experimental Plume Measurements," JANNAF 13th Plume Technology Meeting, Houston, TX, CPIA Publication 357, April 1982, pp. 143–148.